Lithos 358–359 (2020) 105403

Contents lists available at ScienceDirect

Lithos

journal homepage: www.elsevier.com/locate/lithos

Research Article

The earliest Jurassic A-type rhyolites and high-Mg andesites–dacites in southern Jiangxi Province, southeast China: Evidence for delamination of a flat-slab?

Wei-Guang Zhu [a,*], Hong Zhong [a,b], Xing Chen [c], Hui-Qing Huang [d], Zhong-Jie Bai [a], Jun-Hua Yao [a,b], Yan-Jun Wang [a,b], Peng-Cheng Hu [a,b]

[a] State Key Laboratory of Ore Deposit Geochemistry, Institute of Geochemistry, Chinese Academy of Sciences, 99 West Lincheng Road, Guiyang 550081, China
[b] University of Chinese Academy of Sciences, Beijing 100049, China
[c] 264 Brigade of the Jiangxi Nuclear Industry Geological Bureau, Ganzhou 341000, China
[d] Economic Geology Research Center, College of Science and Engineering, Division of Tropical Environments and Societies, James Cook University, Townsville, QLD 4811, Australia

ARTICLE INFO

Article history:
Received 10 May 2019
Received in revised form 19 January 2020
Accepted 25 January 2020
Available online 28 January 2020

Keywords:
Zircon U—Pb ages
Sr–Nd–O–Hf isotopes
Geochemistry
Early Jurassic
Felsic volcanic rocks
Southeastern China

ABSTRACT

Early Jurassic igneous rocks are abundant in the Nanling Range, southeastern China. They are closely related with economically significant deposits, but the tectonic-magmatic controls on their formation are still controversial. This paper reports zircon U–Pb–Hf–O isotopes for the rhyolites, and whole-rock major–trace element and Sr—Nd isotope compositions for the rhyolites and andesites/dacites in the Changpu and Dongkeng basins located in the southern part of Jiangxi Province. The Changpu and Dongkeng rhyolites have high K_2O contents (4.1–7.6 wt%) and K_2O/Na_2O ratios (> 1). Both groups are enriched in HFSE, LREE and show pronounced Nb–Ta–Eu–Sr–P–Ti negative anomalies. Geochemically, they can be classified as A-type and are similar to A_2-type granitoids globally. Their highly evolved whole-rock Sr—Nd isotopes and elevated zircon $\delta^{18}O$ (Changpu rhyolites: $(^{87}Sr/^{86}Sr)_i$ = 0.7140 to 0.7156, $\varepsilon_{Nd}(t) = -7.2$ to -8.7, $\delta^{18}O$ = 8.76 to 9.93‰; Dongkeng rhyolites: $(^{87}Sr/^{86}Sr)_i$ = 0.7149 to 0.7162, $\varepsilon_{Nd}(t) = -6.4$ to -7.9, $\delta^{18}O$ = 7.04 to 9.78‰) are consistent with their generation dominated by remelting of exisiting crustal materials in an extensional environment. The slightly more radiogenic zircon Hf isotopes of the Dongkeng rhyolites, $\varepsilon_{Hf}(t) = -2.1$ to -7.1 as compared with -6.1 to -8.3 of Changpu rhyolites, likely signify some mantle contribution. The Changpu high-Mg andesites–dacites are geochemically similar to high-Mg andesites (HMAs) of the Setouchi arc volcanic belt in Japan and the Piip Volcanos in the western Aleutian Arc. They have very low $\varepsilon_{Nd}(t)$ from -7.8 to -11.3 and highly radiogenic $(^{87}Sr/^{86}Sr)_i$ values from 0.7143 to 0.7154. Similar to HMAs in Setouchi, we suggest that they may be derived from melting of subducted sediments and followed by melt-mantle interaction.

SIMS zircon U—Pb dating yielded extrusive ages of ~190 Ma for both Changpu and Dongkeng rhyolites. The new dating results constrain the minimum age of extrusion of rhyolites and andesites-dacites from the same volcanic sequence to be the earliest Jurassic period. Igneous rocks of this age have very limited distribution in south China. While those found in the coastal regions show features similar to arc rocks, these in the hinterland are rift related. We propose that formation of the Early Jurassic A-type rhyolites and high-Mg andesites–dacites may provide evidence for foundering/delamination of a previously subducted oceanic plateau beneath southeastern China.

1. Introduction

Mesozoic igneous rocks, dominated by abundant granitoids with subordinate mafic intrusions/extrusions, are widespread in southeastern China (Fig. 1a). These magmatic rocks are temporally and spatially associated many world class Sn—W, U, and REE deposits. They have been intensively investigated to gain insights into the ore formation and tectono-magmatic processes in the Mesozoic South China (Zhou et al., 2006; Zhou and Li, 2000). It has been proposed that the magmatism was a response to subduction of the Paleo-Pacific oceanic plate beneath the South China Block during the Mesozoic time (Jahn et al., 1990). However, timing of the initial subduction and the interaction between the subducted oceanic crust and South China continental crust remain subjects of hot debate (Zhou et al., 2006; Zhou and Li, 2000).

Many studies have attributed Triassic magmatism in south China to Indosinian orogeny which was proposed to record the collision between Indochina and South China blocks (Li et al., 2006; Li and Li, 2007). Jurassic granites, or the so-called "Early Yanshanian" granites in many

* Corresponding author.
E-mail address: zhuweiguang@vip.gyig.ac.cn (W.-G. Zhu).

https://doi.org/10.1016/j.lithos.2020.105403
0024-4937/

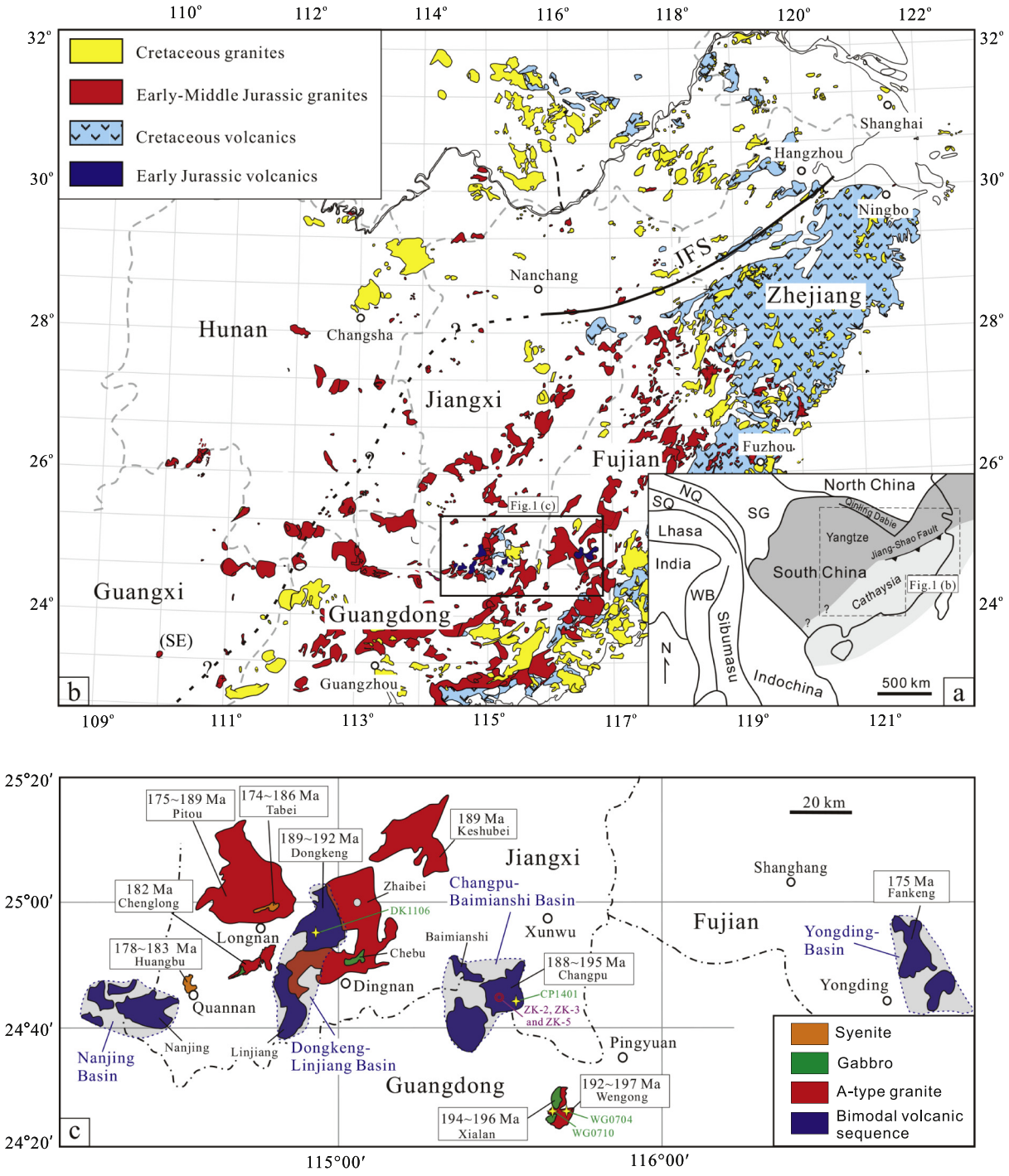

Fig. 1. (a) The map shows major tectonic units and location of Southeastern China (after Metcalfe, 2013). JSF: Jiangshan–Shaoxing Fault. (b) Distribution of the Jurassic–Cretaceous igneous rocks in Southeastern China (modified after Zhou et al., 2006; Cen et al., 2016). (b) Distribution of E–W trend Early Jurassic volcanic and intrusive rocks in South China (modified after 1:200,000 geological map; Cen et al., 2016). Grey fields show the early Jurassic volcanic–sedimentary basins in southern Jiangxi and southwestern Fujian Provinces. Asterisks represent sample locations. Data sources: Pitou granites from Chen et al. (2005) and He et al. (2010); Keshubei granites from Li and Li (2007); Chenglong gabbros from He et al. (2010); Xialan gabbros and Wengong granites from Yu et al. (2010), Zhu et al. (2010), and Gan et al. (2017a, 2017b); Tabei synites from Chen et al. (2005) and He et al. (2010); Huangbu synites from He et al. (2010); Dongkeng and Changpu bimodal volcanic rocks from Ji and Wu (2010) and Cen et al. (2016); Yongding bimodal volcanic rocks from Zhou et al. (2005).

Chinese literatures, are the most abundant in the hinterland of southeastern China. They are dominantly biotite granites emplaced at ca. 160 Ma. And the magmatic calm period from the Late Triassic to the Early Jurassic has been interpreted to record a transition in tectonic regimes from Indosinian collision to the southwest to Paleo-Pacific subduction to the east-southeast (Zhou et al., 2006; Zhou and Li, 2000). It was suggested that subduction of paleo-Pacific oceanic plate only started in Early-Middle Jurassic (Zhou et al., 2006) or Cretaceous (Chen et al., 2008). Alternatively, Li and Li (2007) proposed, on the basis of a comprehensive analysis of the spatial-temporal evolution of metamorphism, magmatism and sedimentary basins that the paleo-Pacific oceanic subduction initiation may be as early as Permian. They

suggested that Jurassic magmatism in South China hinterland may be a response to the delamination of a previously subducted oceanic plateau although there may be ongoing subduction along the coastal region since the earliest Jurassic (Li et al., 2012).

Associated with the voluminous Jurassic granites in the E–W trending igneous belt in the Nanling Range, there are some bimodal volcanic rocks (basalts and rhyolites) preserved in a few small Jurassic basins (Fig. 1a–b; Li et al., 2003, 2007; Chen et al., 2005; Wang et al., 2005; He et al., 2010; Meng et al., 2012; Cen et al., 2016). Some of these bimodal volcanic rocks, as well as a few gabbros and A-type granites have been dated at ca. 190 Ma (e.g., Cen et al., 2016; Gan et al., 2017a, 2017b; Yu et al., 2010; Zhu et al., 2010). Despite volumetrically minor, the few Early Jurassic magmatic records likely hold key to unravelling the tectonic processes in the region. In this paper, we report bulk-rock geochemical and Sr—Nd isotopic results of a suite of newly-discovered andesites/dacites and associated rhyolites in Changpu and Dongkeng basins in southern Jiangxi Province. Zircon U—Pb dating constrained the age of extrusion to be >190 Ma. These earliest Jurassic intermediate rocks are geochemically similar to high-MgO andesites (HMA) in Setouchi, Japan and may present evidence for melting of subducted sediments, hence lending support for subduction before Jurassic.

2. Geological background and petrography

The South China Block (SCB) is bounded to the west and southwest by the Tibetan Plateau and Indochina Block, and to the north by the Qinling-Dabie orogenic belt (Zhou et al., 2006). The SCB consists of the Yangtze Block to the northwest and the Cathaysia Block to the southeast, separated by the Jiangshan–Shaoxing Fault (Fig. 1a–b; Cen et al., 2016). The basement rocks of the Cathaysia Block are mid-Paleoproterozoic (2.0–1.8 Ga) meta-sedimentary rocks (gneiss, amphibolite and migmatite) and granites, which are overlain by Sinian to Triassic sedimentary rocks (Chen and Xing, 2016; Li et al., 2000; Yu et al., 2009).

Mesozoic igneous rocks, such as abundant granites and volcanic rocks, and subordinate gabbros and syenites, are widespread in southeastern China (Fig. 1b; e.g., Zhou and Li, 2000; Wang et al., 2005; Zhou et al., 2005; He et al., 2010; He and Xu, 2012; Cen et al., 2016). These rocks are temporally related to three orogenic episodes, i.e. the Triassic (Indosinian), Jurassic (Early Yanshanian) and Cretaceous (Late Yanshanian) episodes (e.g., Li, 2000; Zhou and Li, 2000; Zhou et al., 2006; Li et al., 2007) (Fig. 1b). The Jurassic igneous rocks occur mainly in the Nanling Range, extending for 500-km-long with E–W trending (Fig. 1b–c; Li et al., 2003, 2007; Chen et al., 2005; Wang et al., 2005;

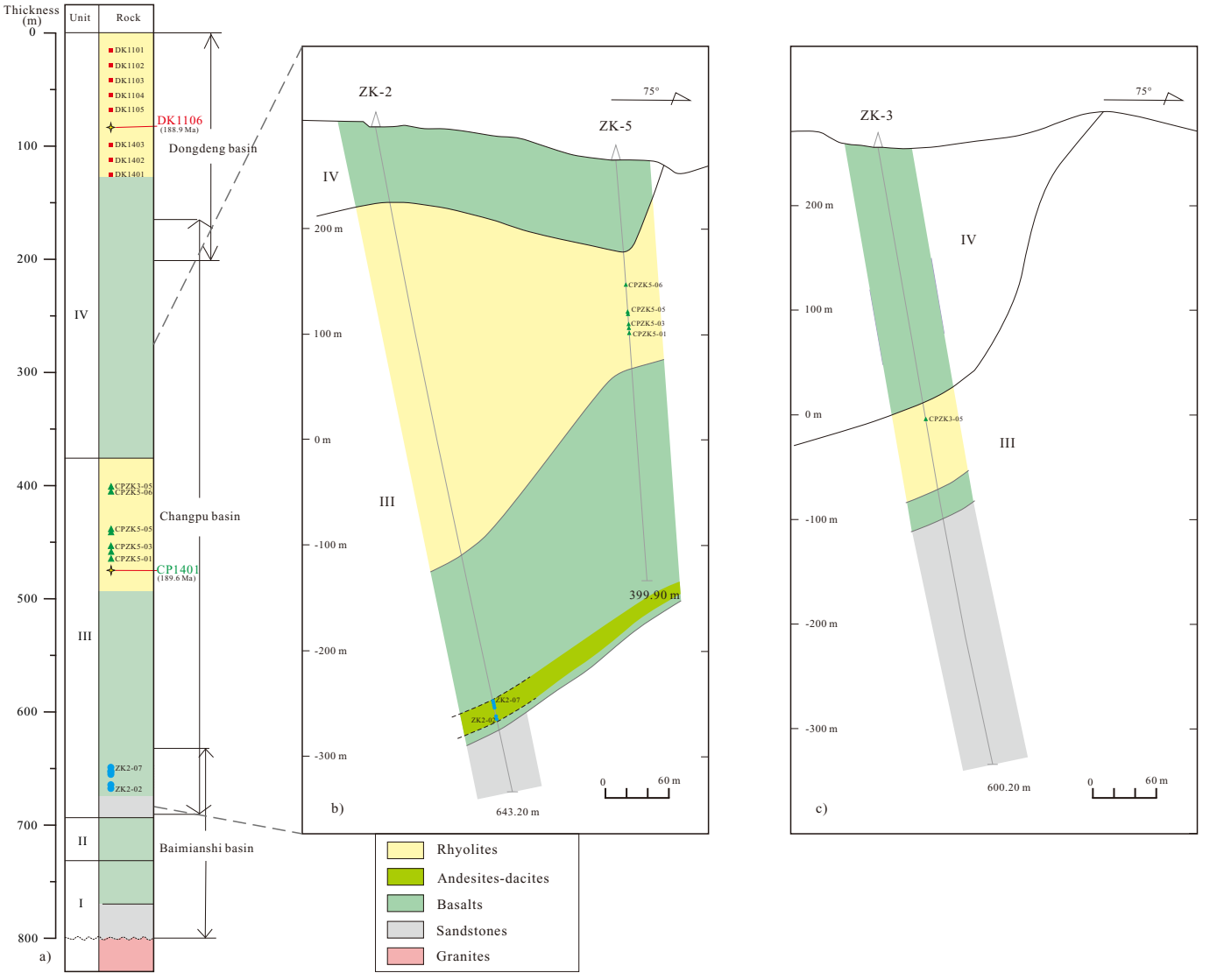

Fig. 2. (a) Simplified stratigraphic columns of the Changpu Formation from the Changpu–Baimianshi and Dongkeng basins; (b) the cross section and sampling sites on the boreholes ZK-2 and ZK-5; and (c) the borehole ZK-3 of the Changpu basin in southern Jiangxi Province, which includes basalts, rhyolites and andesites-dacites.

He et al., 2010; Meng et al., 2012; Cen et al., 2016). The Cretaceous igneous rocks mainly occur to the southeast in the coastal region (Fig. 1a; Zhou and Li, 2000; Zhou et al., 2006; He and Xu, 2012).

The Jurassic bimodal volcanic/intrusive rocks are mainly composed of A-type granites and volcanic rocks (basalts and rhyolites), with subordinate syenites and gabbros (Fig. 1c; Zhou and Li, 2000; Wang et al., 2003, 2005; Zhou et al., 2006; He et al., 2010). They are best exposed in the region from southern Hunan, through southern Jiangxi and northern Guangdong, to southwestern Fujian (Fig. 1a–b; Li et al., 2003; Chen et al., 2005; Zhou et al., 2005; He et al., 2010; Yu et al., 2010; Zhu et al., 2010; Meng et al., 2012; Cen et al., 2016). The Jurassic volcanic rocks are preserved in the Nanjing, Dongkeng–Linjiang and Changpu–Baimianshi basins in the southern part of Jiangxi Province, and the Yongding basin in southwestern part of Fujian Province (Fig. 1c). In the Dongkeng–Linjiang and the Changpu–Baimianshi basins, the volcanic-sedimentary sequence of the Jurassic Yutian Group consists of the Shuitoujing Formation (J_1sh) and the Changpu Formation (J_1ch) from bottom to top. The Shuitoujing Formation (J_1sh) is mainly composed of sandstones with conglomerate interlayers and has a total thickness of >200 m. It unconformably overlies Precambrian metamorphic rocks, Paleozoic sedimentary rocks and Triassic granites (Wu et al., 2000). The overlying Changpu Formation (J_1ch) is >800 m in thickness and composed predominantly of basalts, rhyolites, and sandstones, plus minor high-Mg andesites–dacites (Fig. 2a; Wu et al., 2000; Zhang et al., 2002; Wang et al., 2003, 2005). The main volcanic-sedimentary sequence of the Changpu Formation (J_1ch) from bottom to top can be divided into four cyclic units (Unit I to Unit IV; Fig. 2a) on the basis of the appearance sandstones or basalts. The Changpu and Dongdeng rhyolites are from the upper parts of Unit III and Unit IV, respectively (Fig. 2a–c). The discovered andesite and dacite samples were a layer of ~20 m in thickness interbedded within the lower part of Unit III basalts in the Changpu basin (Fig. 2b). The Rb—Sr isochron ages of the volcanic rocks are between ~180–160 Ma (Zhang et al., 2002). The SHRIMP zircon U—Pb isotope ages of the rhyolites in the Changpu basin and the dacites of the Dongkeng basin were 195 Ma and 191 Ma, respectively (Ji and Wu, 2010). The LA–ICP–MS zircon U—Pb isotope ages of the rhyolites in the Changpu and Dongkeng basins are ~190–188 Ma (Cen et al., 2016).

Fifteen rhyolite samples were collected from several outcrops and two drill cores (ZK-3 and ZK5) in the Changpu and Dongkeng basins (Fig. 1c, 2b–c). These rocks are phyric, containing abundant medium- to fine-grained phenocrysts of quartz (~10–15 vol%), plagioclase (2–5%), K-feldspar (2–5%). The plagioclase and K-feldspar phenocrysts had undergone moderate alteration. The groundmass is mainly composed of very fine-grained plagioclase and quartz (Fig. 3a, b). The andesite and dacite samples used in this study were collected from one drill core (ZK-2) in the Changpu basin (Fig. 2b). These rocks contain ~3–5 vol% of medium-grained quartz phenocrysts and very fine-grained clinopyroxene and plagioclase assemblages, and Fe—Ti oxides (magnetite and ilmenite) in the groundmass. Most clinopyroxene and plagioclase grains have been partially altered to uralite and epidote (Fig. 3c, d).

3. Analytical methods

Zircons were separated from two large rhyolite samples, one from the Changpu basin (CP1401; Fig. 1c, 2a) and the other from the Dongkeng basin (DK1106; Fig. 1c, 2a), using conventional heavy liquid and magnetic techniques, followed by handpicking under a binocular microscope. The zircon grains were mounted in an epoxy resin disc, polished, and coated with gold. Cathodoluminescence (CL) images were used to select the undeformed grains with regular zoning and without visible inherited cores for dating. The U, Th and Pb concentrations and isotope compositions were determined using a CAMECA IMS-1280 SIMS at the Institute of Geology and Geophysics, Chinese Academy of Sciences in Beijing, China. Detailed analytical procedure is similar to that of Li et al. (2009b). The size of the ion beam is about

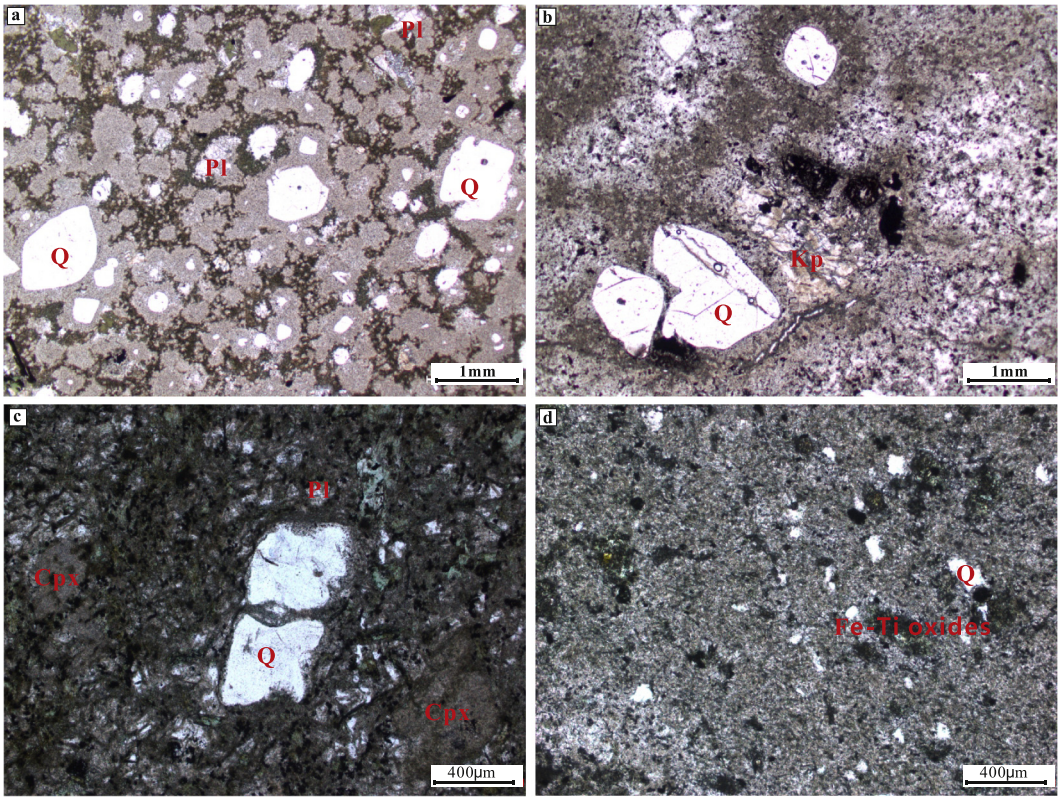

Fig. 3. Photographs of representative rhyolites and andesites-dacites from the Changpu and Dongkeng basins: (a) rhyolite (CP1401), (b) rhyolite (DK1106), (c) andesite (ZK2–03), and (d) dacite (ZK2–04). Mineral abbreviations: Q = quartz, Pl = plagioclase, Kp = K-feldspar, Cpx = clinopyroxene.

20 × 30 μm. The reported isotopes are after correction for common Pb using non-radiogenic ^{204}Pb. The measured isotopes are reported for 1σ confidence (~90%). The calculated ages are reported for 2σ confidence (~95%). Data reduction was carried out using the Isoplot/Ex v. 2.49 program (Ludwig, 2001). The Qinghu zircon standard analyzed with our samples yield an U—Pb age of 163.4 ± 5.6 Ma, indistinguishable from the recommended value (Li et al., 2013).

Zircon oxygen isotopic analysis was also conducted using a CAMECA 1280 SIMS at the Institute of Geology and Geophysics, Chinese Academy of Sciences in Beijing, China. A ~ 20 μm ion beam was used for the analysis. Detailed operating conditions and analytical procedure are similar to those of Li et al. (2009b, 2013). The uncertainty for each analysis is generally better than 0.3–0.4‰ (2SE). The Penglai and Qinghu zircon standards were used for calibration and quality control, respectively. The reported $^{18}O/^{16}O$ values are after correction for the IMF, and reported after normalization to the Vienna Standard Mean Ocean Water compositions (VSMOW, $^{18}O/^{16}O = 0.0020052$). The Qinghu zircon standard measured together with our samples has a mean $\delta^{18}O = 5.50 \pm 0.21$‰ (2SE), similar to the recommended value of 5.4 ± 0.2‰ (2SE) (Li et al., 2013).

Zircon Lu—Hf isotopic analysis was performed using a Nu Plasma MC-ICP-MS equipped with a UP-213 laser-ablation system in the State Key Laboratory of Environmental Geochemistry, Institute of Geochemistry, Chinese Academy of Sciences, Guiyang, China, following the analytical procedures of Tang et al. (2008). The obtained weighted mean $^{176}Hf/^{177}Hf$ ratio of the zircon standard 91,500 is 0.282306 ± 31 (2σ, n = 27), in good agreement with the recommended value (0.282306 ± 10, 2σ, Woodhead et al., 2004). The initial $^{176}Hf/^{177}Hf$ ratios were calculated based on the measured $^{176}Hf/^{177}Hf$ ratios and the decay constant of ^{176}Lu of 1.867×10^{-11} yr^{-1} (Söderlund et al., 2004). The ε_{Hf} values were calculated using the chondritic ratios of $^{176}Hf/^{177}Hf = 0.282772$ and $^{176}Lu/^{177}Hf = 0.0332$ (Blichert-Toft and Albarede, 1997) and the obtained age for the zircons. The single-stage model ages (T_{DM1}^{Hf}) were calculated using the model of depleted mantle with a present-day $^{176}Hf/^{177}Hf$ ratio of 0.28325 and $^{176}Lu/^{177}Hf = 0.0384$ (Griffin et al., 2002). The two-stage model ages (T_{2DM}^{Hf}) were calculated assuming that the average continental crust has a mean $^{176}Lu/^{177}Hf$ value of 0.015 (Griffin et al., 2002).

Major element compositions of whole rocks were determined by X-ray fluorescence method at the analytical laboratory of the ALS Chemex Co Ltd. in Guangzhou, China. Certified reference materials (NIM-GBW07105, GBW07163, GBM908–10, and MRGeo08) were used as the standards. The analytical precision is generally better than 5%. The concentrations of trace elements in whole rocks were analyzed using a Perkin-Elmer Sciex ELAN DRC-e ICP-MS at the State Key Laboratory of Ore Deposit Geochemistry, Institute of Geochemistry, Chinese Academy of Sciences (IGCAS), Guiyang, China. Powdered samples (50 mg) were dissolved using HF + HNO_3 mixture in high-pressure Teflon bombs at

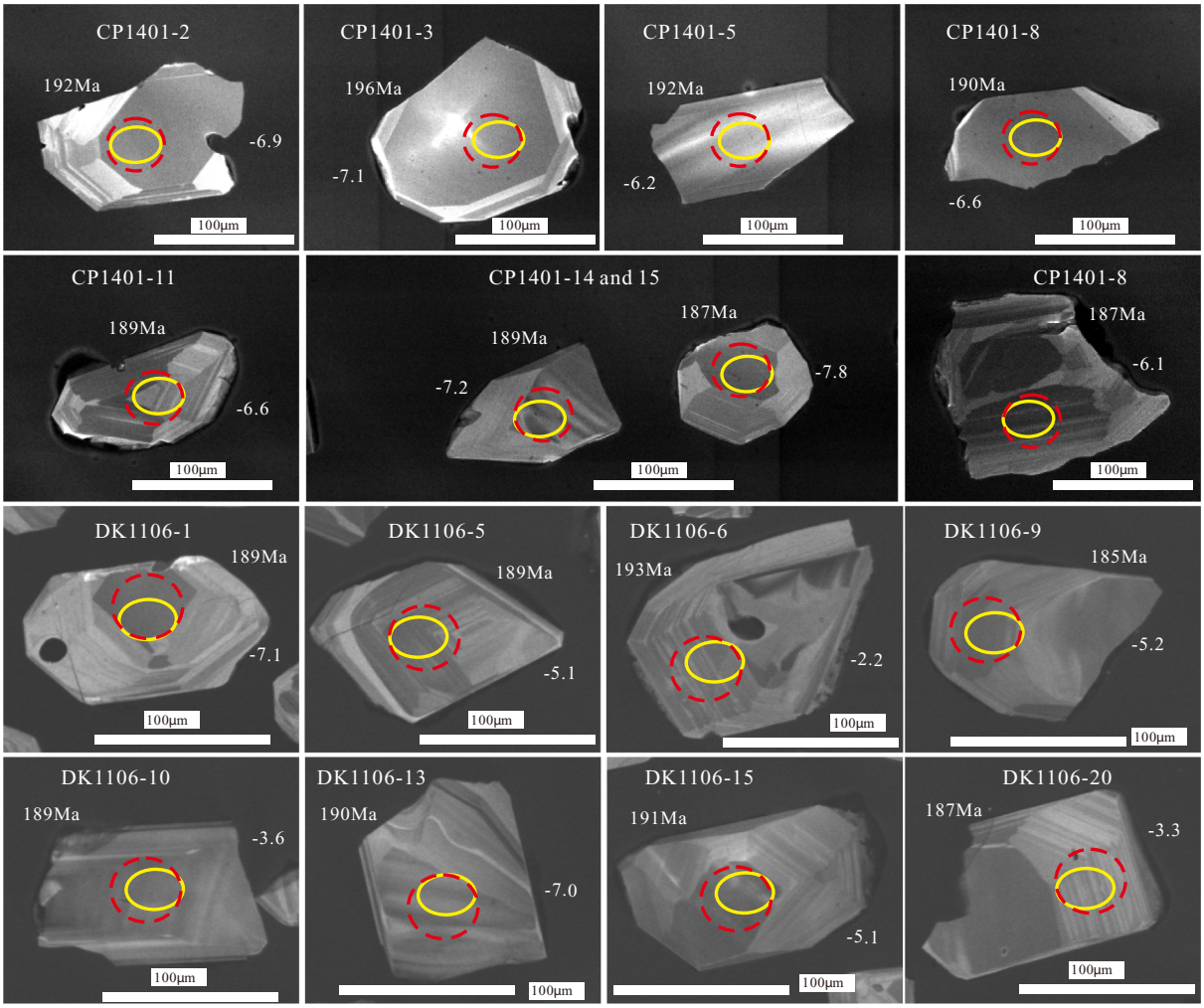

Fig. 4. Representative cathodoluminescence (CL) images of zircon grains from Changpu and Dongkeng rhyolites (CP1401 and DK1106). The ellipses with yellow solid lines are for U—Pb analysis points and the circles with red dash lines are for Hf isotope analysis points.

~190 °C for 48 h (Qi et al., 2000). Rh was used to monitor signal drift during ICP-MS analysis. International reference materials (BHVO-2 and BCR-2) were used as the standards. The analytical precision is generally better than 10%.

To prepare for Sr—Nd isotope analysis, the powered volcanic rock samples were spiked and dissolved in Teflon bombs with HF-HNO_3-$HClO_4$ mixture. The sample solutions were used for element separation in the conventional cation-exchange columns. The element concentration and isotope measurements were performed using an MC–ICP–MS in the State Key Laboratory of Environmental Geochemistry, Institute of Geochemistry, Chinese Academy of Sciences, Guiyang, China. The reported $^{87}Sr/^{86}Sr$ and $^{143}Nd/^{144}Nd$ ratios are after correction for mass fractionation based on $^{86}Sr/^{88}Sr = 0.1194$ and $^{146}Nd/^{144}Nd = 0.7219$. The $^{86}Sr/^{88}Sr$ ratio of the NBS987 Sr standard, analyzed together with our samples is 0.710250 ± 7 (2σ); the $^{143}Nd/^{144}Nd$ ratios of the USGS standard BCR-2 and the JNDI-1 Nd standard, determined together with our samples, are 0.512629 ± 16 (2σ) and 0.512119 ± 14 (2σ), respectively. These values are in good agreement with the recommended values.

4. Analytical results

4.1. Zircon U—Pb ages of the Changpu and Dongkeng rhyolites

The selected zircons extracted from a rhyolite sample (CP1401) from the Changpu basin (Fig. 1c) are euhedral and transparent, with oscillatory zoning (Fig. 4). They are up to 100- to 150-μm long, with the length-to-width ratios between 1:1 and 2:1. The analytical results show variable concentrations of U (117–258 ppm) and Th (81–267 ppm), with the Th/U ratios from 0.65 to 1.03 for these zircons (Supplemental Table A). The measured U—Pb isotopes for these grains yield a weighted mean $^{206}Pb/^{238}U$ age of 190 ± 1.3 Ma (Fig. 5a).

The selected zircons from a rhyolite sample (DK1106) from the Dongkeng basin (Fig. 1c) are mostly euhedral grains with concentric zoning (Fig. 4). The sizes of the zircons are from 50 to 100 μm in width, with the length to width ratios between 1:1 and 2:1. They contain U from 170 to 413 ppm and Th from 85 to 306 ppm, with Th/U ratios between 0.40 and 0.81 (Supplemental Table A). The weighted mean of $^{206}Pb/^{238}U$ age of these zircons is 189 ± 1.3 Ma (Fig. 5b).

4.2. Zircon Hf—O isotopes of the Changpu and Dongkeng rhyolites

The Hf and O isotopes of the dated zircons are listed in Supplemental Table B. The $\varepsilon_{Hf}(t)$ values and two-stage model ages (T^{Hf}_{2DM}) were calculated using their U—Pb isotope ages given above. The zircon grains from a rhyolite sample (CP1401) from the Changpu basin (Fig. 1b) display a limited range of $\varepsilon_{Hf}(t)$ values between −6.1 and − 8.3, with the two-stage Hf model ages (T^{Nd}_{2DM}) of 1.61–1.75 Ga (Fig. 4, 6a–b). Their $\delta^{18}O$ values are from 8.76 to 9.93‰ (Supplemental Table B; Fig. 6b).

The $\varepsilon_{Hf}(t)$ values of the zircons from a rhyolite sample (DK1106) from the Dongkeng basin (Fig. 1b) vary from −2.1 to −7.1, with the two-stage Hf model ages (T^{Hf}_{2DM}) of 1.36 to 1.68 Ga (Supplemental Table B; Fig. 4, 6a–b). The $\delta^{18}O$ values of these zircon grains are from 7.04‰ to 9.78‰ (Supplemental Table B; Fig. 6b), slightly lower than those of the selected zircon grains from the Changpu rhyolites (sample CP1401).

4.3. Whole-rock elemental and Sr—Nd isotopic compositions

4.3.1. Major and trace element compositions

The results for eight samples of rhyolites and six samples of andesites/dacites from the Changpu basin, and nine samples of rhyolites from the Dongkeng basin are listed in Table 1. The major oxides described below are the recalculated values on a LOI-free basis (LOI = loss on ignition). The Changpu rhyolites are characterized by high SiO_2 and $Fe_2O_3^T$ contents (SiO_2 = 72.6–76.4%, $Fe_2O_3^T$ = 3.54–6.87%). The abundances of other major oxides are MgO = 0.20–0.57%, TiO_2 = 0.36–0.55%, Al_2O_3 = 11.7–13.4%, CaO = 0.60–3.01%, and P_2O_5 = 0.05–0.14% (Table 1, Fig. 7). The Dongkeng rhyolites have larger ranges of major oxides, with SiO_2 from 66.1% to 77.5%, $Fe_2O_3^T$ from 3.11% to 8.27%, MgO from 0.14% to 1.57%, TiO_2 from 0.33% to 1.32%, Al_2O_3 from 11.0% to 15.3%, CaO from 0.03 to 2.68%, and P_2O_5 from 0.06% to 0.30% (Table 1 and Fig. 7). The rhyolites from both basin all contain very low Cr (2.91–33.4 ppm) and Ni (1.46–10.4 ppm) (Table 1), show a weak negative correlation between SiO_2 and other oxides such as MgO, TiO_2, $Fe_2O_3^T$, Al_2O_3, CaO, and P_2O_5 (Fig. 7). The rhyolites display high total alkali and K_2O contents ($Na_2O + K_2O$ = 4.52–8.00%, K_2O = 4.09–7.60%, Na_2O = 0.10–3.66%, and K_2O/Na_2O = 1.12–43.0) and plot in the subalkaline series with rock types varying from dacite to rhyolite (Fig. 8a; Le Bas and Streckeisen, 1991). On the K_2O versus SiO_2 diagram (Fig. 8b; Rickwood, 1989), these rocks plot in the fields of both high-K calc-alkaline and shoshonitic series. Their A/CNK and A/NK values are from 0.89 to 1.88 and from 1.19 to 2.71, plotting in the peraluminous field (Fig. 9a). The observed negative correlation between P_2O_5 and SiO_2 contents (Fig. 7f) appears to be inconsistent with the compositions of typical S-type granitoids (Chappell, 1999). On the other hand, their high MALI values ($Na_2O + K_2O$-CaO = 3.14–7.82%; Fig. 9b) and high $Fe_2O_3^T$ contents coupled by high ($FeO^T/(FeO^T + MgO)$ ratios

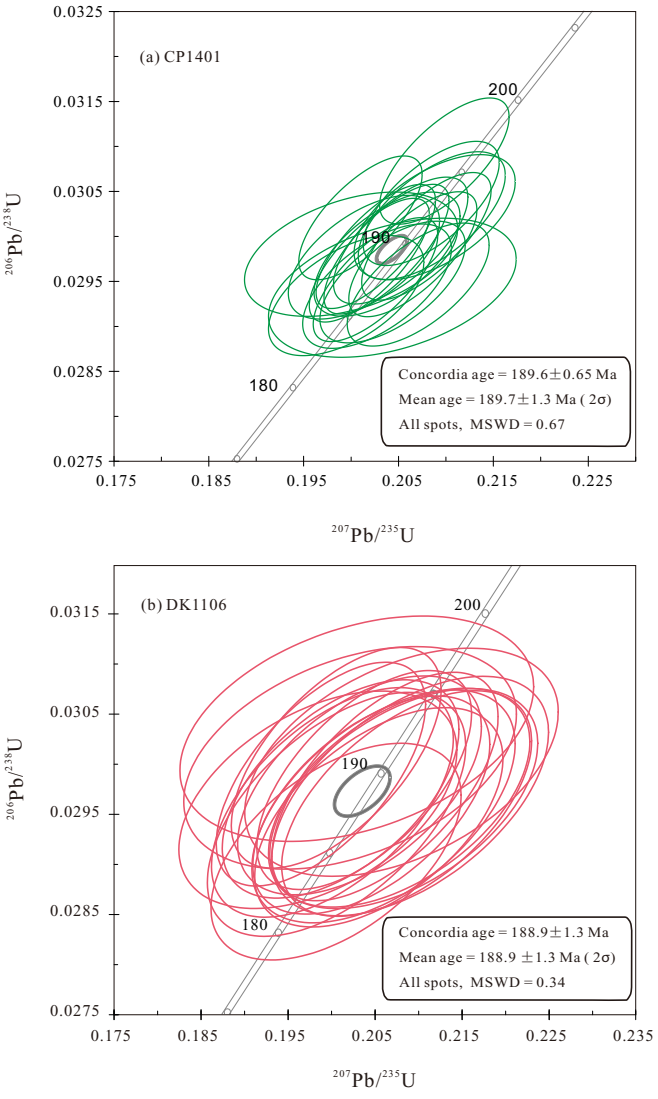

Fig. 5. SIMS zircon U—Pb concordia diagrams for (a) sample CP1401 and (b) sample DK1106 of the rhyolites from the Changpu and Dongkeng basins.

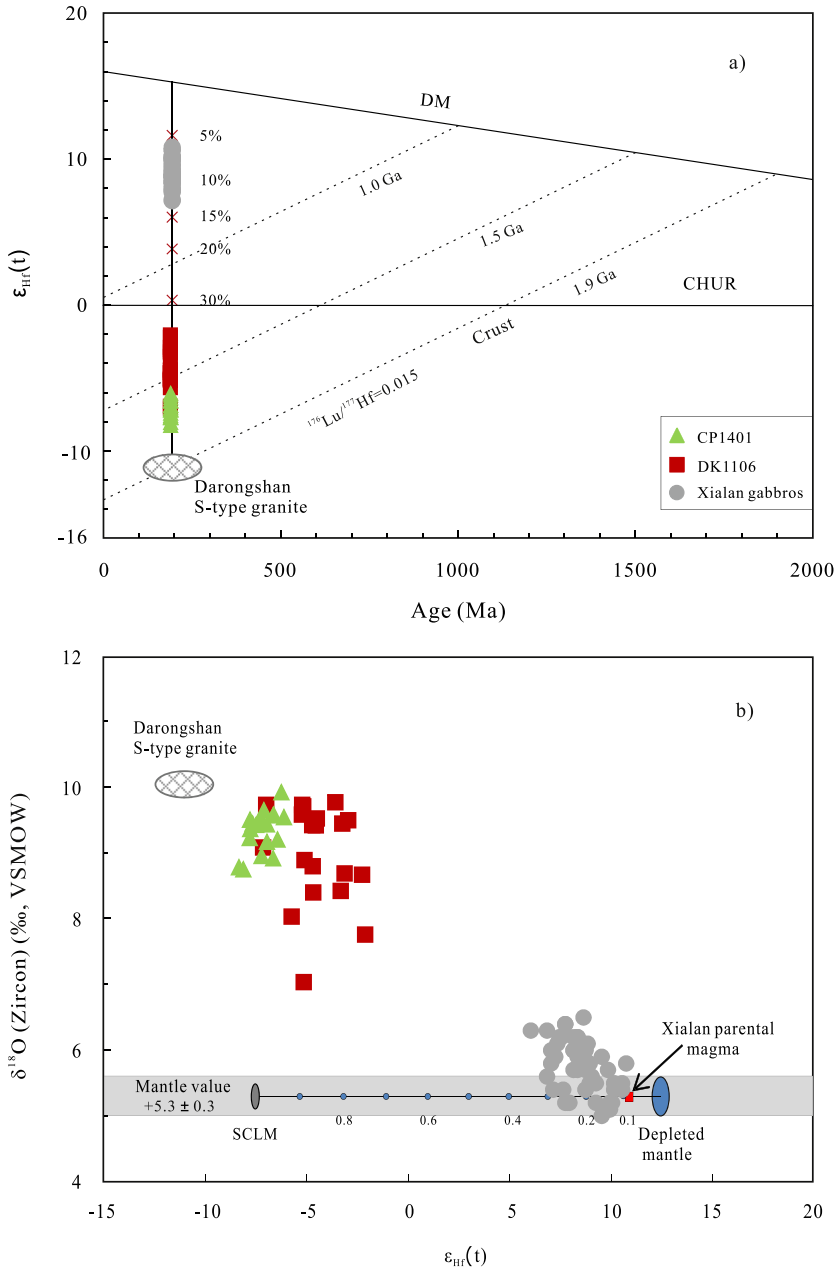

Fig. 6. (a) Plot of zircon ε_{Hf} values versus U—Pb ages and (b) plot of zircon $\delta^{18}O$ values versus ε_{Hf} values for the rhyolites from the Changpu and Dongkeng basins. The assumed asthenosphere (depleted mantle) compositions are $\varepsilon_{Hf} = 12.5$ and $\delta^{18}O = 5.3‰$. The assumed subcontinental lithospheric mantle (SCLM) compositions are $\delta^{18}O = 5.3‰$ and $\varepsilon_{Hf} = -7.5$, which is the same as the value calculated using the equation of $\varepsilon_{Hf} = 1.33\varepsilon_{Nd} + 3.19$ for $\varepsilon_{Nd} = -8.0$ (Vervoort and Blichert-Toft, 1999) and $\delta^{18}O = 5.3‰$. The assumed upper crustal melt compositions are $\varepsilon_{Hf} = -11$ and $\delta^{18}O = 10‰$, which are similar to the values of zircons from S-type Daronghe granites in the region (Jiao et al., 2015;Qi et al., 2007; Yu et al., 1999). Data sources: zircon U—Pb ages for the Xialan gabbros are from Zhu et al. (2010); zircon Hf—O isotopes for the Xialan gabbros are from Bai et al. (2015).

(0.77–0.96; Fig. 9c) are consistent with the compositions of typical A-type granitoids (e.g.,Eby, 1992 ; Whalen et al., 1987).

The Changpu andesites–dacites have moderate contents of SiO_2 (60.4–68.7%) and TiO_2 (0.53–1.04%), high $Mg^{\#}$ values (51–59), high MgO (2.23–7.50%), $Fe_2O_3^T$ (4.19–10.6%), Al_2O_3 (14.0–16.1%) concentrations (Table 1, Fig. 7, 8c-d), plus moderate abundances of compatible trace elements such as Cr (138–303 ppm) and Ni (37.2–97.5 ppm) (Table 1). On the Harker diagrams (Fig. 7), the MgO, TiO_2, Fe_2O_3, P_2O_5, Cr and Ni contents of the andesites–dacites decrease with increasing SiO_2 contents whereas the Al_2O_3 contents show the opposite relation with SiO_2. The andesites–dacites also display relatively high total alkalis and K_2O contents ($Na_2O + K_2O$ = 3.75–5.86%, K_2O = 2.43–4.26%, Na_2O = 0.36–2.20%, and K_2O/Na_2O = 1.58–9.60) (Fig. 8a, b). On the ($Na_2O + K_2O$) vs. SiO_2 diagram, these rocks plot in the subalkaline series, encompassing the andesite and dacite fields (Fig. 8a; Le Bas and Streckeisen, 1991). They belong to the high-K calc-alkaline and shoshonitic series based on the K_2O-SiO_2 classification of Rickwood (1989) (Fig. 8b). The high MgO contents and $Mg^{\#}$ values, coupled by moderate SiO_2 contents meet the definition of high-Mg andesites (HMAs) according to Kelemen et al. (2003). On the SiO_2 vs. MgO (Fig. 8c; McCarron and Smellie, 1998; Liu et al., 2018) and $Mg^{\#}$ vs. SiO_2 diagrams (Fig. 8d; Liu et al., 2018), the samples plot within or very close to the HMAs field. Notably, the Changpu andesites/dacites have higher TiO_2 concentrations ($TiO_2 > 0.5\%$) than those of the typical boninitic HMAs (Fig. 10a; Le Bas and Streckeisen, 1991; Tang and Wang, 2010).

The Changpu and Dongkeng rhyolites have relatively high rare earth element (REE) contents (ΣREE = 209–615 ppm). In the chondrite-normalized REE spider diagram (Fig. 11a), the rhyolites exhibit

Table 1
Major element (in wt%) and trace element (in ppm) data for the rhyolites and andesites–dacites from the Changpu and Dongkeng basins.

Changpu basin							
Sample no.	CP1401	CPZK3–05	CPZK5–01	CPZK5–02	CPZK5–03	CPZK5–04	CPZK5–05
Rock type	Rhyolite	Rhyolite	Rhyolite	Rhyolite	Rhyolite	Rhyolite	Rhyolite
SiO_2	70.40	71.10	71.80	71.40	71.00	71.60	72.50
TiO_2	0.53	0.45	0.38	0.39	0.40	0.39	0.41
Al_2O_3	11.25	13.05	12.20	12.05	12.00	12.00	12.00
$Fe_2O_3^T$	4.51	6.69	4.93	5.21	5.42	5.27	5.04
MnO	0.09	0.08	0.15	0.09	0.12	0.12	0.06
MgO	0.55	0.45	0.21	0.31	0.33	0.25	0.24
CaO	2.90	1.16	1.02	0.89	0.89	0.99	0.59
Na_2O	1.60	0.10	3.60	1.96	1.77	2.02	1.40
K_2O	4.32	4.30	4.02	5.55	5.81	5.74	6.51
P_2O_5	0.13	0.06	0.07	0.07	0.08	0.08	0.08
LOI	3.50	2.95	1.29	1.46	1.57	1.61	1.29
Total	99.78	100.39	99.67	99.38	99.39	100.07	100.12
$Mg^{\#}$	19.5	11.8	7.8	10.5	10.8	8.6	8.6
Sc	11.5	7.34	7.16	6.96	6.87	7.32	7.34
V	4.35	6.02	4.52	6.69	5.92	6.13	6.02
Cr	2.91	4.58	7.98	6.41	5.07	11.10	4.58
Co	4.35	65.1	37.0	37.2	66.4	75.8	65.1
Ni	1.71	4.77	4.40	3.70	4.57	9.04	4.77
Cu	11.9	2.70	2.35	9.73	2.24	2.05	2.70
Zn	114	98.2	80.1	117	102	99.3	98.2
Ga	17.4	21.8	18.2	22.4	20.7	21.6	21.8
Rb	166	215	128	188	200	194	215
Sr	127	88.3	131.0	120	118	99.9	88.3
Y	49.9	47.3	49.7	69.5	76.0	65.0	47.3
Zr	353	569	553	605	573	561	569
Nb	23.1	43.2	40.3	43.6	42.9	43.7	43.2
Cs	1.95	6.52	3.37	6.44	7.05	5.90	6.52
Ba	812	1310	956	1120	1170	1170	1310
La	60.8	101	75.0	100	94.1	88.2	101
Ce	121	189	153	179	175	185	189
Pr	14.1	21.4	16.0	20.3	19.5	18.4	21.4
Nd	55.3	80.7	59.0	78.2	71.9	69.1	80.7
Sm	10.5	14.7	11.5	14.5	14.1	13.4	14.7
Eu	1.63	2.68	2.39	2.63	2.58	2.38	2.68
Gd	9.75	12.5	9.98	13.1	12.9	12.1	12.5
Tb	1.44	1.77	1.64	2.02	2.07	1.96	1.77
Dy	8.35	9.75	9.31	12.5	12.3	11.6	9.75
Ho	1.67	1.85	1.77	2.44	2.53	2.21	1.85
Er	4.81	5.06	5.10	7.07	6.99	6.55	5.06
Tm	0.68	0.71	0.74	1.02	1.05	0.88	0.71
Yb	4.40	4.74	5.15	6.81	6.67	6.18	4.74
Lu	0.60	0.65	0.73	0.94	0.99	0.89	0.65
Hf	9.57	14.3	13.6	14.1	14.6	14.0	14.3
Ta	1.22	1.82	1.62	1.75	1.77	1.83	1.82
Pb	31.7	38.0	31.0	34.3	39.0	36.7	38.0
Th	24.2	30.5	28.0	30.2	29.6	29.6	30.5
U	4.46	1.38	1.46	1.85	1.99	1.44	1.38
T_{Zr} (°C)	800	997	876	912	903	891	912

Sample no.	CPZK5–06	ZK2–02	ZK2–03	ZK2–04	ZK2–05	ZK2–06	ZK2–07	DK1101
Rock type	Rhyolite	Dacite	Andesite	Dacite	Dacite	Dacite	Andesite	Rhyolite
SiO_2	74.90	67.08	57.53	60.30	61.81	61.78	59.07	76.32
TiO_2	0.35	0.52	0.98	0.98	0.84	0.83	0.86	0.33
Al_2O_3	11.45	15.67	14.00	13.72	13.68	13.78	13.64	10.84
$Fe_2O_3^T$	3.47	4.09	10.02	7.61	7.60	7.56	10.24	3.06
MnO	0.03	0.08	0.21	0.12	0.17	0.16	0.14	0.02
MgO	0.20	2.18	7.15	4.35	5.30	5.13	6.26	0.14
CaO	0.92	2.18	1.48	3.03	4.23	4.52	1.76	0.03
Na_2O	2.10	2.15	0.34	0.70	1.58	1.46	0.43	0.25
K_2O	4.54	3.57	3.23	2.99	2.49	2.38	4.13	7.49
P_2O_5	0.05	0.09	0.36	0.34	0.30	0.30	0.31	0.06
LOI	1.54	2.06	4.37	3.99	2.21	2.14	2.82	1.27
Total	99.55	99.67	99.67	98.13	100.21	100.04	99.66	99.81
$Mg^{\#}$	10.2	51.4	58.6	53.1	58.0	57.3	54.8	8.3
Sc	5.24	10.5	30.0	22.7	21.2	18.0	17.1	8.11
V	5.23	63.2	270	196	167	149	232	9.96
Cr	4.37	138	303	146	195	155	293	5.26
Co	67.8	9.14	33.4	25.3	23.3	19.3	27.7	2.01
Ni	5.51	37.5	97.5	37.2	52.5	44.6	49.9	1.46
Cu	1.76	4.20	149	47.8	4.52	4.53	42.1	8.53
Zn	92.8	57.9	117	82.9	100	95.0	93.9	94.5
Ga	16.6	19.0	20.5	18.7	17.6	15.6	17.6	12.8

Table 1 (*continued*)

Sample no.	CPZK5–06	ZK2–02	ZK2–03	ZK2–04	ZK2–05	ZK2–06	ZK2–07	DK1101
Rb	135	195	191	170	118	108	185	225
Sr	98.8	228	65.9	174	366	375	200	61.0
Y	62.6	21.5	43.8	32.8	30	26.2	29.7	31.4
Zr	623	250	154	213	206	198	204	333
Nb	49.8	15.0	14.2	19.2	17.7	17.2	18.0	24.6
Cs	5.99	11.9	17	15.8	13.1	13.7	24.7	4.59
Ba	801	1320	1210	1080	1180	877	1450	990
La	89.0	41.0	47.1	43.6	41.7	39.7	40.1	55.9
Ce	177	79.9	94.9	88.6	83.8	79.8	85.0	107
Pr	19.1	8.95	10.4	10.1	9.49	8.66	9.29	13.2
Nd	71.9	32.9	40.4	38.6	35.6	33.2	36.1	46.5
Sm	13.8	6.42	8.79	7.82	7.20	6.57	7.09	9.01
Eu	2.10	1.61	2.16	1.73	1.52	1.53	1.83	1.73
Gd	12.0	5.08	8.85	6.96	6.27	6.13	7.05	8.71
Tb	1.88	0.73	1.31	1.07	0.97	0.91	1.02	1.22
Dy	11.5	3.82	7.22	5.85	5.34	4.95	5.02	6.04
Ho	2.14	0.72	1.37	1.12	1.02	0.93	1.03	1.30
Er	6.29	1.97	3.58	3.05	2.81	2.59	3.01	3.49
Tm	0.91	0.29	0.50	0.45	0.42	0.38	0.39	0.46
Yb	5.75	1.80	2.89	2.79	2.57	2.36	2.55	3.05
Lu	0.82	0.27	0.42	0.41	0.38	0.32	0.33	0.45
Hf	15.8	6.15	3.95	5.33	5.11	4.67	4.59	9.81
Ta	2.04	1.10	1.00	1.30	1.23	1.17	1.18	1.68
Pb	39.2	14.6	34.0	15.3	21.2	23.9	9.74	11.5
Th	32.8	16.7	14.1	16.2	16.6	15.1	15.0	21.0
U	1.98	3.84	3.42	3.68	3.53	3.38	3.98	5.02
T_{Zr} (°C)	930							868

Dongkeng basin

Sample no.	DK1102	DK1103	DK1104	DK1105	DK1106	DK1401	DK1402	DK1403
Rock type	Rhyolite	Rhyolite	Rhyolite	Rhyolite	Rhyolite	Rhyolite	Rhyolite	Rhyolite
SiO_2	72.91	69.73	72.55	69.44	70.26	67.10	70.40	65.10
TiO_2	0.32	0.52	0.38	0.51	0.40	0.76	0.90	1.30
Al_2O_3	12.79	13.17	11.98	14.78	13.37	13.35	11.60	13.15
$Fe_2O_3^T$	3.35	5.59	4.39	4.88	4.64	5.65	5.09	8.14
MnO	0.02	0.06	0.05	0.03	0.05	0.09	0.06	0.07
MgO	0.17	0.19	0.21	0.32	0.32	1.54	0.78	1.18
CaO	0.81	1.49	1.23	0.11	1.31	2.48	1.24	2.64
Na_2O	2.38	3.04	1.16	1.28	1.23	2.59	0.83	1.24
K_2O	5.34	4.86	5.33	5.27	5.42	4.44	6.61	5.35
P_2O_5	0.07	0.15	0.09	0.10	0.10	0.13	0.23	0.30
LOI	1.22	0.95	2.30	2.58	2.66	1.55	1.17	1.76
Total	99.38	99.75	99.67	99.30	99.76	99.68	98.91	100.23
$Mg^{\#}$	9.1	6.3	8.7	11.5	12.0	35.1	23.3	22.3
Sc	12.8	13.7	9.66	14.0	8.42	13.1	12.8	18.4
V	11.2	18.1	12.8	19.5	15.0	76.2	58.3	73.4
Cr	7.04	7.37	7.12	8.44	7.84	33.4	17.6	7.46
Co	1.97	4.17	2.78	3.09	2.82	51.3	52.1	37.0
Ni	2.45	4.81	2.73	2.91	3.49	9.76	10.4	4.82
Cu	6.83	14.1	12.0	17.2	9.04	12.5	10.1	7.46
Zn	102	151	105	142	91.8	89.9	76.4	110
Ga	21.9	25.7	20.2	27.5	22.9	21.0	15.3	23.4
Rb	224	187	231	254	263	200	202	182
Sr	122	90.4	80.0	48.6	78.3	186	140	265
Y	59.2	42.9	34.9	104	41.6	44.8	45.1	61.3
Zr	357	346	315	432	434	352	227	324
Nb	27.7	26.3	27.7	37.1	27.6	24.4	16.1	23.5
Cs	5.66	4.92	7.37	9.47	10.4	5.58	1.50	1.04
Ba	889	669	721	1012	765	784	595	502
La	76.8	58.6	54.0	124.6	63.0	53.2	44.7	61.0
Ce	142	114	107	233	128	109	81.0	117
Pr	18.1	14.3	12.9	29.5	14.9	12.6	9.7	14.3
Nd	67.2	52.9	47.0	118	56.6	48.8	38.4	56.2
Sm	14.1	11.0	9.44	25.7	10.8	9.60	8.43	11.2
Eu	2.36	2.01	1.93	4.47	2.24	1.77	1.39	1.88
Gd	13.7	10.6	9.39	27.9	11.0	8.36	7.45	10.9
Tb	2.19	1.58	1.38	4.27	1.54	1.37	1.19	1.68
Dy	11.09	8.34	7.15	21.4	8.08	7.90	7.22	9.93
Ho	2.40	1.79	1.52	4.33	1.56	1.44	1.39	1.99
Er	6.08	4.65	3.91	10.7	4.28	4.01	3.94	5.50
Tm	0.84	0.63	0.52	1.36	0.60	0.60	0.54	0.73
Yb	5.21	4.04	3.47	8.27	3.86	3.60	3.41	4.58
Lu	0.73	0.58	0.50	1.18	0.58	0.51	0.48	0.67
Hf	10.9	10.7	9.68	12.9	11.0	9.57	5.98	8.64

(*continued on next page*)

Table 1 (*continued*)

Dongkeng basin								
Sample no.	DK1102	DK1103	DK1104	DK1105	DK1106	DK1401	DK1402	DK1403
Ta	2.04	1.81	1.89	2.47	1.86	1.55	1.09	1.42
Pb	36.0	33.6	31.8	35.8	25.5	27.1	23.2	28.5
Th	29.5	28.0	24.1	29.5	25.3	21.7	16.6	23.8
U	6.31	6.59	4.77	8.99	7.18	5.02	3.08	4.68
T_{Zr} (°C)	850	814	846	947	895	803	783	802

$Mg^{\#} = 100^{*}$molar MgO/(Mg + FeO^{T}), assuming $FeO^{T} = 0.9 \times Fe_2O_3^{T}$. Total iron as FeO_T. T_{Zr} is calculated from zircon saturation thermometry (Boehnke et al., 2013). LOI = loss on ignition.

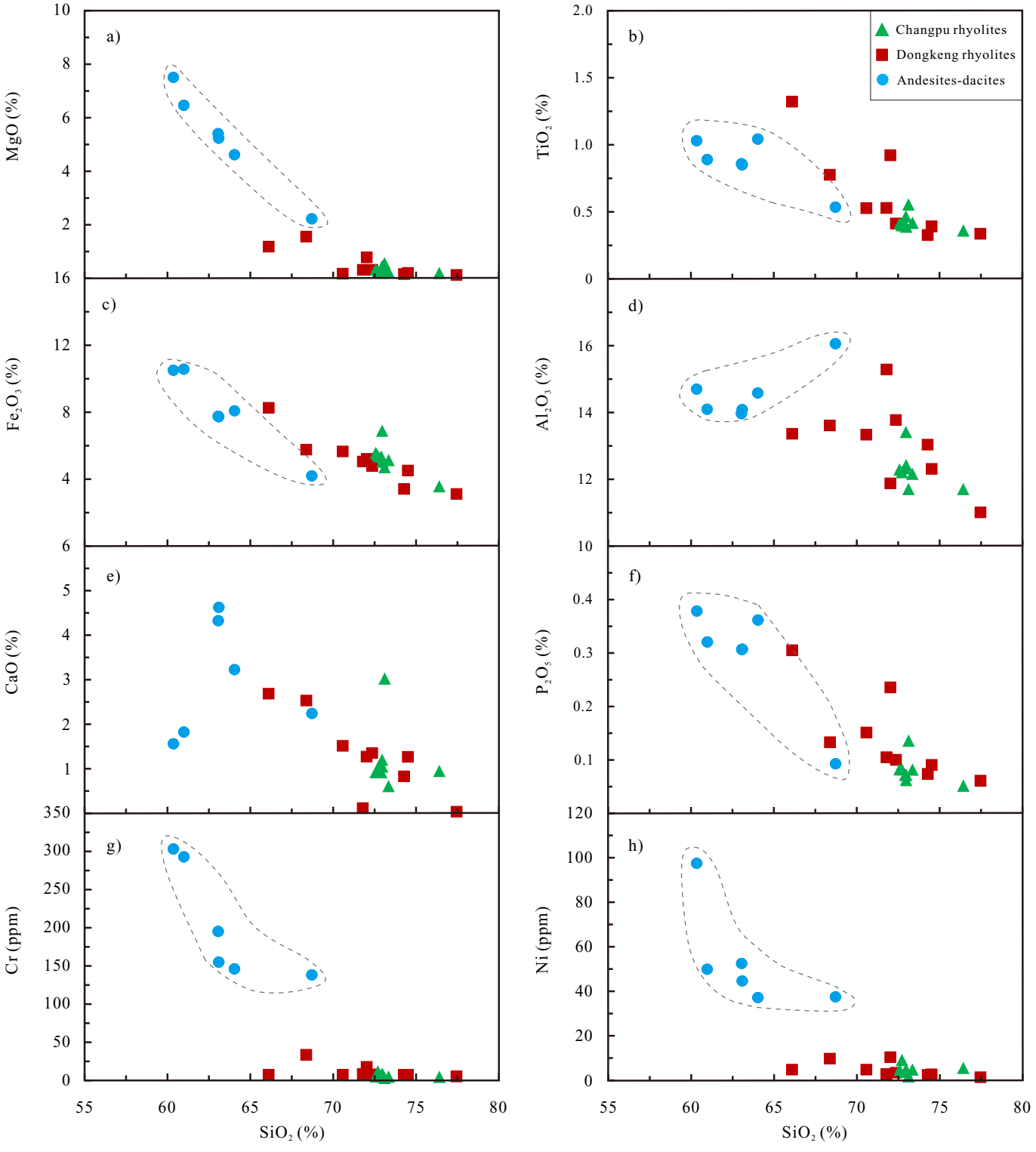

Fig. 7. Selected variation diagrams of major oxide and compatible element (MgO, TiO_2, Fe_2O_3, Al_2O_3, CaO, P_2O_5, Cr and Ni) contents and silica for the rhyolites and andesites–dacites from the Changpu and Dongkeng basins.

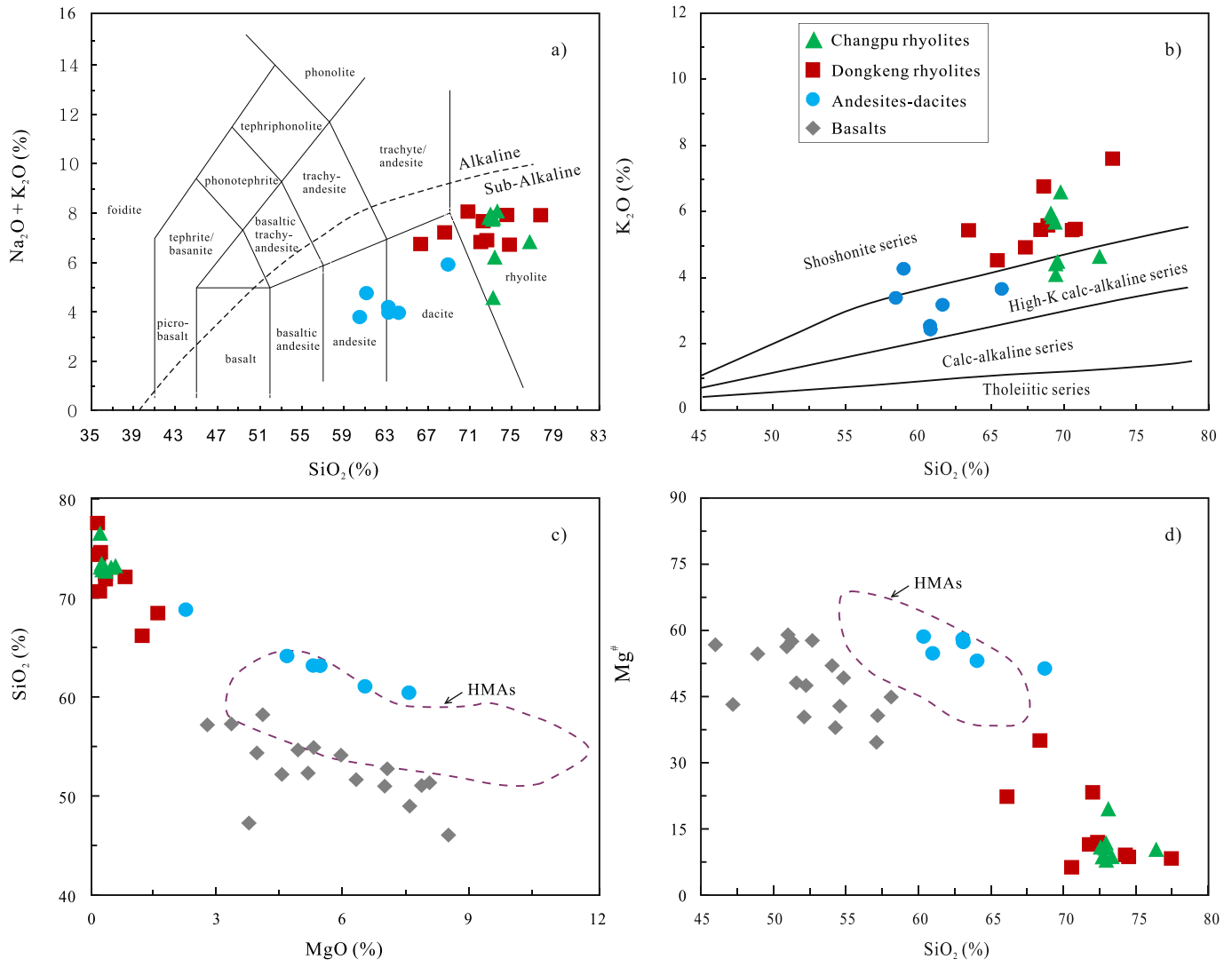

Fig. 8. (a) ($Na_2O + K_2O$) vs. SiO_2 classification diagram (Le Bas and Streckeisen, 1991); (b) K_2O vs. SiO_2 diagram (Rickwood, 1989); (c) SiO_2 vs. MgO diagram (Liu et al., 2018; McCarron and Smellie, 1998); and (d) $Mg^{\#}$ vs. SiO_2 diagram (Liu et al., 2018) for the rhyolites and andesites–dacites from the Changpu and Dongkeng basins. Data sources: Major elemental data (SiO_2, MgO, and $Mg^{\#}$) of Early Jurassic Jiangxi basalts from Wang et al. (2005) and Cen et al. (2016).

significant light REE enrichments plus negative Eu anomalies (Eu/Eu* = 0.49–0.68). In the primitive mantle-normalized incompatible trace element spider diagram (Fig. 11b; Sun and McDonough, 1989), the rhyolites show distinctly negative Nb-Ta-Sr-P-Ti anomalies. The rhyolites are also characterized by high contents of Ga, Nb, Zr, REE, and Y (Ga = 12.8–27.5 ppm, Nb = 16.1–49.8 ppm, Zr = 227–623 ppm, REE = 209–615 ppm, and Y = 31.4–104 ppm), plus low Sr contents (48.6–265 ppm) (Table 1). The Zr + Nb + Ce + Y contents in these rocks range from 369 ppm to 912 ppm, higher than the average values of typical A-type granitoids (Zr + Nb + Ce + Y > 350 ppm; Whalen et al., 1987). The 10,000 × Ga/Al ratios of the rhyolitic rocks range from 2.19 to 3.64. On the diagram of Zr versus Ga/Al (Fig. 12a), these rocks all plot in the field of A-type granitoids (Eby, 1992; Whalen et al., 1987). According to the geochemical subdivision of A-type granitoids of Eby (1992), the rhyolites plot in the field of A_2-type granitoids (Fig. 12b). The calculated zircon saturation temperatures (T_{Zr}) for the Changpu and Dongkeng rhyolites are from 800 to 997 °C and 783–947 °C, respectively (Table 1; Boehnke et al., 2013).

The Changpu andesites–dacites have moderate contents of REE (ΣREE = 185–230 ppm) and show light REE-enrichments in the chondrite-normalized REE spider diagram (Fig. 11c), plus slightly negative Eu anomalies (Eu/Eu* = 0.69–0.86). In the primitive mantle-normalized incompatible trace element spider diagram (Fig. 11d; Sun and McDonough, 1989), the andesites–dacites are characterized by significant enrichment in some large-ion lithophile elements (LILEs) such as Ba and depletion in some high field strength elements (HFSEs) such as Nb, Ta, Ti and P (Fig. 11d). On the $(La/Yb)_{CN}$ vs. Yb_{CN} diagram (Fig. 10b; Tang and Wang, 2010) and the Sr/Y vs. Y diagram (Fig. 10c; Tang and Wang, 2010), the andesites–dacites are very similar to the Cenozoic high-Mg andesites (HMA) from the Volcanic Belt (SVB) of the Setouchi arc in SW Japan (Shimoda et al., 1998; Tatsumi, 2001) and the Late Pliocene (?) and Pleistocene-Holocene HMAs from the Piip Volcanos of the Far Western Aleutian island arc (Yogodzinski et al., 1994). On the other hand, the Changpu andesites–dacites are significantly different from the Adak-type rocks and the boninitic HMAs (Fig. 8b–c; Tang and Wang, 2010).

4.3.2. Sr—Nd isotope compositions

Whole-rock Sr—Nd isotope compositions of the andesites/dacites and rhyolites in the Changpu and Dongkeng basins are given in Table 2. The Sr—Nd isotope compositions the Changpu rhyolites are very similar to those of the Dongkong rhyolites. The initial $(^{87}Sr/^{86}Sr)_i$

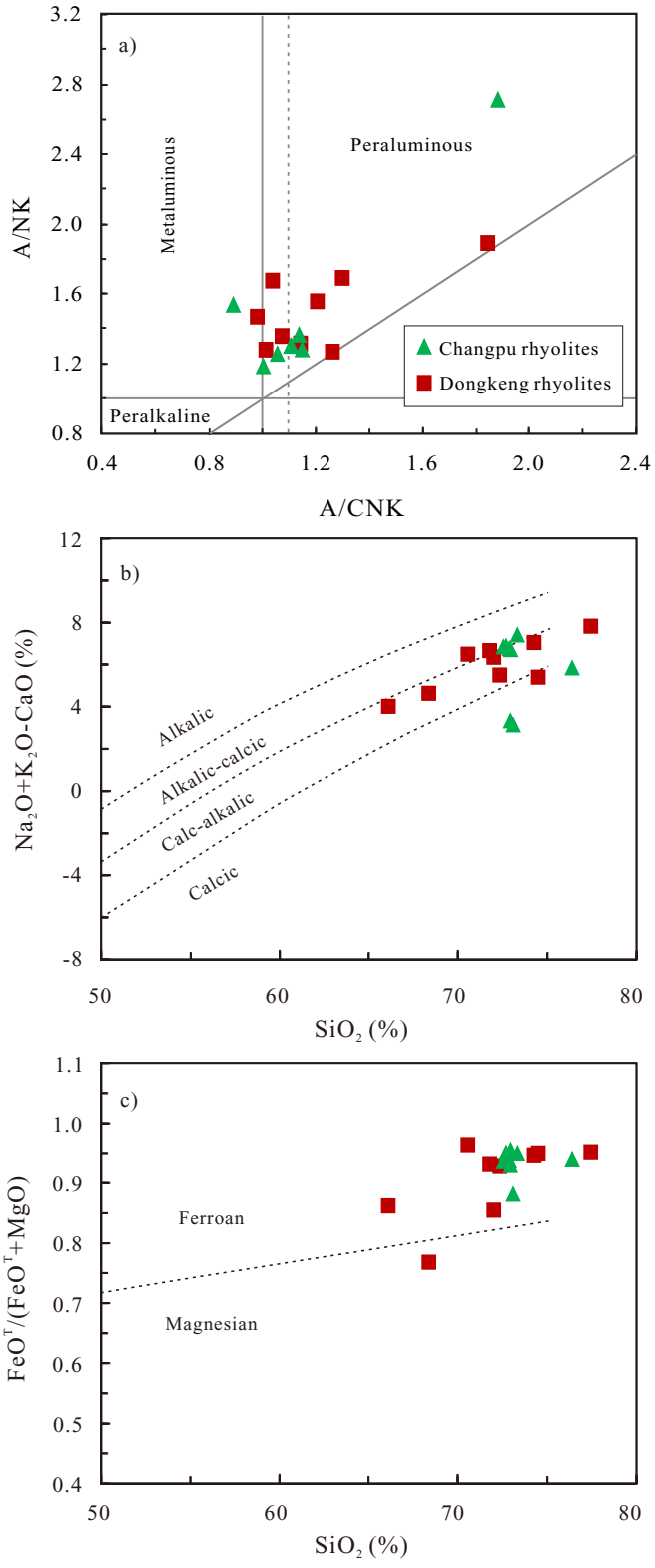

Fig. 9. Plots of (a) A/NK vs. A/CNK, (b) ($Na_2O + K_2O$-CaO) (modified alkali lime index) vs SiO_2, (c) $FeO^T/(FeO^T + MgO)$ (Fe-index) vs SiO_2 of the rhyolites from the Changpu and Dongkeng basins. A/NK = molar ratio $Al_2O_3/(Na_2O + K_2O)$, A/CNK = molar ratio $Al_2O_3/(CaO + Na_2O + K_2O)$.

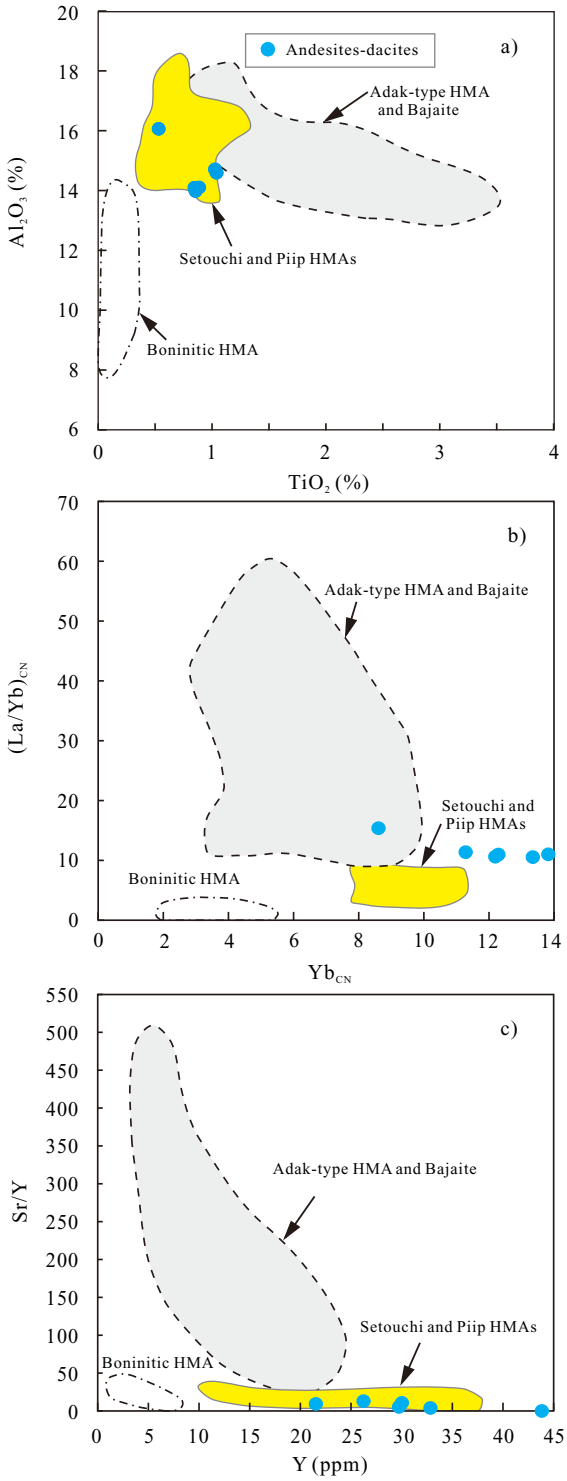

Fig. 10. Plots of (a) Al_2O_3 vs.TiO_2 (Tang and Wang, 2010), (b) $(La/Yb)_{CN}$ vs.Yb_{CN} (Tang and Wang, 2010), and (c) Sr/Y vs. Y (Tang and Wang, 2010) of the Changpu andesites–dacites.

ratios and the $\varepsilon_{Nd}(t)$ values of the Changpu rhyolites range from 0.7140 to 0.7156 and from −7.2 to −8.7, the two-stage Nd model ages (T^{Nd}_{2DM}) between 1.38 and 1.49 Ga (Table 2 and Fig. 13). The Dongkeng rhyolites have the initial $(^{87}Sr/^{86}Sr)_i$ ratios from 0.7149 to 0.7162_and the ε_{Nd} (t) values from −6.4 to −7.9, with the two-stage Nd model ages (T^{Nd}_{2DM}) from 1.30 to 1.40 Ga (Table 2; Fig. 13).

The Changpu andesites and dacites have a small range of $^{143}Nd/^{144}Nd$ ratios between 0.51196 and 0.51216, with the ε_{Nd} (t) values from −7.8 to −11.3 and the two-stage Nd model ages (T^{Nd}_{2DM}) between 1.40 and 1.69 Ga. The andesites and dacites have highly variable $^{87}Sr/^{86}Sr$ ratios from 0.71681–0.73708, with the initial $(^{87}Sr/^{86}Sr)_i$ ratios ranging from 0.7143 to 0.7154 (Table 2 and Fig. 13).

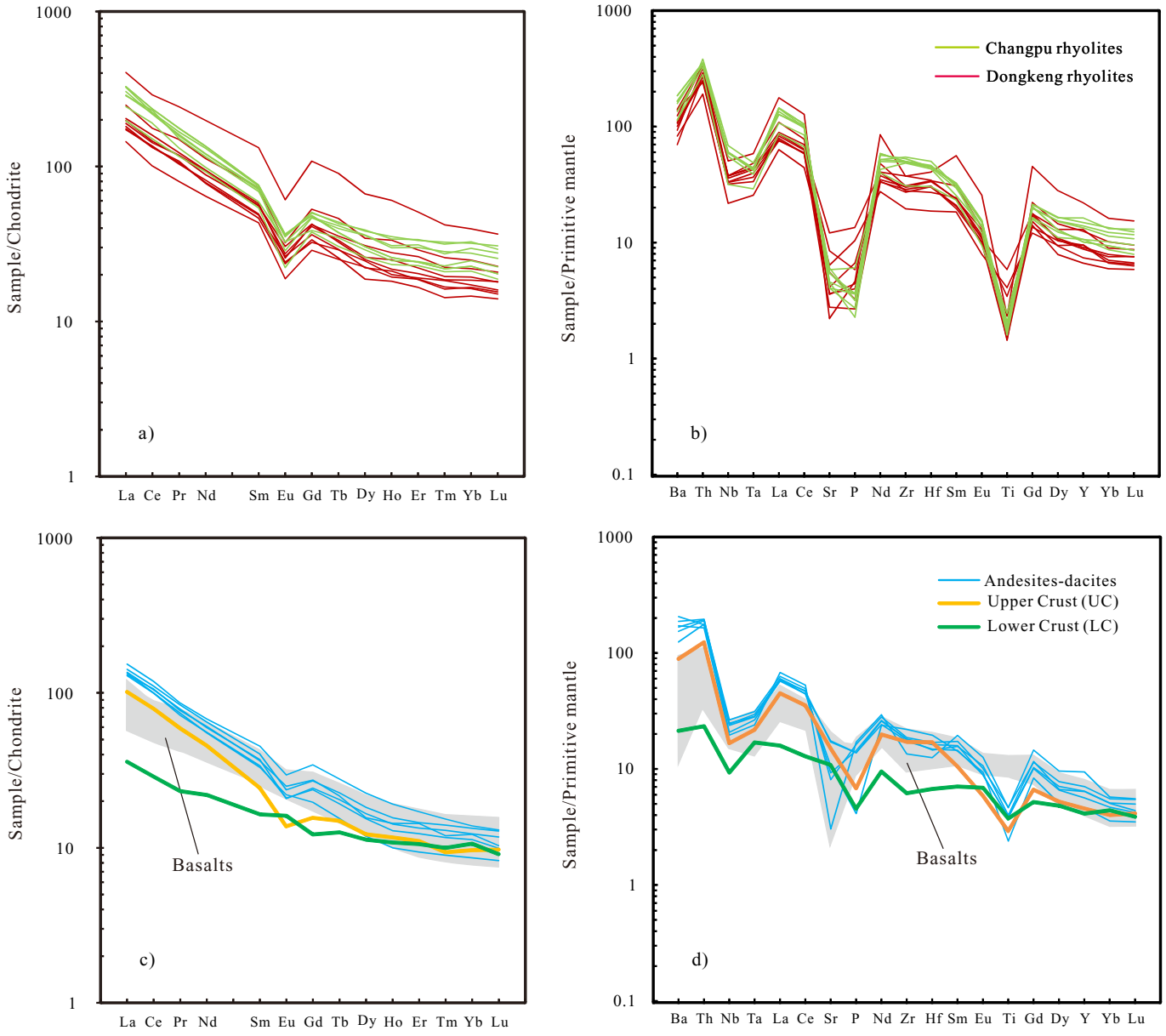

Fig. 11. Chondrite-normalized REE diagrams and primitive mantle-normalized incompatible trace element multi-element plot for the Changpu and Dongkeng rhyolites (a, b) and the Changpu andesites–dacites (c, d), recpectively. Chondrite-normalizing values are from Boynton (1984). Primitive mantle-normalizing values are from Sun and McDonough (1989). Data sources: Trace element of upper crust (UC) and lower crust (LC) from Rudnick and Gao (2003); Trace elemental data of Early Jurassic Jiangxi basalts from Cen et al. (2016).

5. Discussion

5.1. Timing of the volcanism in the Changpu and Dongkeng basins

The new CAMECA SIMS zircon U—Pb dating results from this study reveal that the rhyolites in the Changpu and Dongkeng basins were erupted at ~ 190 Ma and 189 Ma, respectively (Fig. 5a, b), consistent with published LA–ICP–MS zircon U—Pb dating results (190–188 Ma; Cen et al., 2016). The age data show that the volcanic-sedimentary sequence composed of the rhyolites and basalts in the Changpu and Dongkeng basins were erupted quickly in the earliest Jurassic period. Although the apparent age of the volcanism is slightly younger than that of the Xialan gabbros (~194 Ma) and the Wengong granites (~192 Ma) in the region (Zhu et al., 2010), they are indistinguishable with an error of 1%. Therefore, we consider that these magmatism were coeval.

5.2. Petrogenesis of the A-type Changpu and Dongkeng rhyolites

Several petrogenetic models have been proposed for the A-type granitoids: (1) extensive fractional crystallization of basaltic magma with or without crustal assimilation (Turner et al., 1992), (2) partial melting of anhydrous crustal rocks (Huang et al., 2011; Whalen et al., 1987), or (3) mixing between mantle- and crustal-derived magmas (Kerr and Fryer, 1993; Yang et al., 2007). The Changpu and Dongkeng rhyolites have low $\varepsilon_{Nd}(t)$ values (−6.4 to −8.7) and high $(^{87}Sr/^{86}Sr)_i$ (0.7140–0.7162) (Fig. 13), which are significantly different from those of the associated basalts ($\varepsilon_{Nd}(t) = +0.27$ to -4.8, $(^{87}Sr/^{86}Sr)_i = 0.7047$ to 0.7102) (Fig. 13; Wang et al., 2005; Cen et al., 2016) and the coeval Xialan gabbros ($\varepsilon_{Nd}(t) = +1.7$ to $+6.2$, $(^{87}Sr/^{86}Sr)_i = 0.7041$ to 0.7060) (Fig. 13; Zhu et al., 2010). The dramatic differences indicate that the rhyolites and the coeval mafic rocks in the region do not share a common source and are not related to each other simply by fractional crystallization.

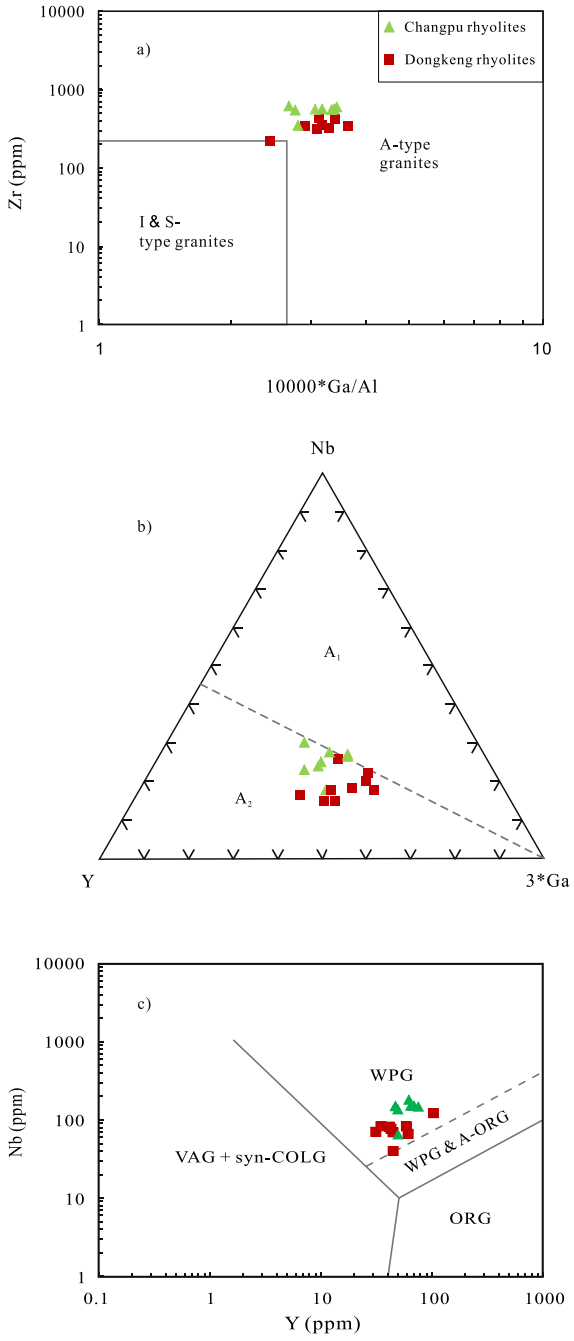

Fig. 12. (a) Zr versus 10,000 × Ga/Al diagram (Eby, 1992) showing the rhyolites from the Changpu and Dongkeng basins are affinitive to A-type granites; (b) Nb–Y–Ga ternary diagram (Eby, 1992) for the subdivision of A_1- and A_2-type granites showing the Changpu and Dongkeng rhyolites are affinitive to A_2-type granites; and (c) Nb versus Y diagram (Pearce et al., 1984) showing that the Changpu and Dongkeng rhyolites are plotted exclusively into the field of within-plate granites (WPG). Abbrviations: VAG = volcanic arc granites; *syn*-COLG = syn-collisional granites; WPG = within-plate granites; ORG = ocean ridge granites.

Zircon Hf—O isotopic data are useful for detecting the involvement of different source components during magma generation including magma mixing (e.g., Griffin et al., 2002; Kemp et al., 2007; Valley et al., 2005). Zircons of the igneous rocks that formed from mantle-derived magma without significant crustal contamination or formed from the partial melts of a mafic crust originally formed from such mantle-derived magma are characterized by mantle-like $\delta^{18}O$ values (e.g., Valley et al., 2005). The $\delta^{18}O$ values of zircons crystallizing from typical mantle-derived magma is 5.3 ± 0.3‰ (2σ; Valley et al., 2005). This value increases with increasing amount of crustal contamination (e.g. Eiler, 2001; Li et al., 2009a). The zircon $\delta^{18}O$ values of >7.5‰ are commonly attributed to melting or assimilation of a supracrustal source, e.g., altered volcanic rocks or sedimentary rocks (e.g., Huang et al., 2011; Valley et al., 2005). The $\varepsilon_{Hf}(t)$ and $\delta^{18}O$ values of zircons from the Changpu rhyolites (sample CP1401) are down to −8.3 and up to +9.93‰, respectively, which are very close to the values for the Triassic Darongshan S-type granites thought to have formed from melting of buried supracrustal rocks (Fig. 6b; Yu et al., 1999; Qi et al., 2007; Jiao et al., 2015). This seems to suggest that the Changpu rhyolites also formed dominantly by crustal melting. However, the negative correlation between the zircon $\delta^{18}O$ and $\varepsilon_{Hf}(t)$ indicates that a small mantle component may also have been involved in their formation (Fig. 6b).

Compared to the zircons of the Changpu rhyolites, the zircons of the Dongkeng rhyolites (sample DK1106) have higher $\varepsilon_{Hf}(t)$ values (−2.1 to −7.1) but lower $\delta^{18}O$ values (+7.04 to +9.78‰) The two stage Nd and Hf model ages of the Dongkeng rhyolites are slightly younger (T^{Nd}_{2DM} = 1.30–1.41 Ga, T^{Hf}_{2DM} = 1.36–1.68 Ga) than those of the Changpu rhyolites. As shown in Fig. 6a–b, these differences can be explained by higher proportion of mantle-derived component in the Dongkeng rhyolites.

The chemical compositions of the Changpu and Dongkeng rhyolites vary from dacitic to rhyolitic (Fig. 8a). The variation is consistent with variable degrees of fractional crystallization in the magma chamber (Fig. 7). The negative correlation between their SiO_2 contents and the contents of other oxides such as MgO, TiO_2, Fe_2O_3, Al_2O_3, CaO and P_2O_5 may result from fractionation of Mg-Fe-Ca-Al-Ti-P rich minerals, such as pyroxenes, alkali feldspars, plagioclase, Fe—Ti oxides and apatite. Fractionation of these minerals can also explain strong negative anomalies of Eu, Ba, Sr, P and Ti as shown in the primitive mantle normalized trace element distribution patterns (Fig. 11a–b).

5.3. Petrogenesis of the Changpu high-Mg andesites–dacites

High-Mg andesites and associated rocks in the world could have formed in different ways, such as (1) melts are extracted from a harzburgite residue (e.g., Wood and Turner, 2009), (2) partial melting of the overlying lower continental crust or (e.g., Gao et al., 2004; Xu et al., 2002), (3) mixing between mantle- and crust-derived magmas (e.g., Qian and Hermann, 2010; Streck et al., 2007), and (4) interaction of melts from the subducting slab (the oceanic crustal materials or the subducted sediments) and the overlying mantle (e.g., Liu et al., 2018; Shimoda et al., 1998; Tatsumi, 2001; Zeng et al., 2016). Below we use the geochemical and isotopic data to explore which process may have led to the formation of these high-Mg andesites-dacites in the Early Jurassic South China.

The Changpu high-Mg andesites and dacites have Nd—Sr isotope compositions ($\varepsilon_{Nd}(t)$ = −7.8 to −11.3, $(^{87}Sr/^{86}Sr)_i$ = 0.7143–0.7154) significantly different from those of the coeval mantle-derived gabbros and basalts, but similar to coeval rhyolites and Middle–Late Jurassic granites in the region (Fig. 13). Additionally, they are enriched in Th (14.1–16.7 ppm) and U (3.4–4.0 ppm). These features rule out the possibility that the high-Mg andesites/dacites would have formed from direct mantle melting. The correlation between MgO, SiO_2 and ε_{Nd} (t) (Fig. 14a–b) shows that it cannot from by mixing of coeval mantle-derived melts with crust or crustal-derived magmas, either.

As is shown in Fig. 10, the Changpu high-Mg andesites-dacites are similar to the HMAs of the Setouchi Arc Volcanic Belt (Shimoda et al., 1998; Tatsumi, 2001) and the Piip Volcanos in the Western Aleutian Island Arc (Yogodzinski et al., 1994). They are also characterized by low U/Th (Fig. 15a), Th/La (Fig. 15b) and Ba/Th (Fig. 15c) ratios, implying a significant contribution from sediments. Like HMAs in Setouchi, these features along with enrichment in Th and U lead us to conclude that the Changpu high-Mg andesites-dacites were derived from melting of sediments (Turner et al., 1996), melts of which were then assimilated in mantle to achieve the high-MgO characters (Tatsumi, 2001).

Table 2
Sr and Nd isotopic data for the rhyolites and andesites–dacites from the Changpu and Dongkeng basins.

Sample no.	Rb (ppm)	Sr (ppm)	$^{87}Rb/^{86}Sr$	$^{87}Sr/^{86}Sr$	±2σ	$(^{87}Sr/^{86}Sr)_i$	Sm (ppm)	Nd (ppm)	$^{147}Sm/^{144}Nd$	$^{143}Nd/^{144}Nd$	±2σ	$^{143}Nd/^{144}Nd$ (i)	$\varepsilon_{Nd}(t)$	T_{DM}^{Nd} (Ma)	T_{2DM}^{Nd} (Ma)
Changpu rhyolites															
CP1401	166	127	3.79	0.725808	0.000010	0.71563	10.5	55.3	0.115	0.512129	0.000003	0.511987	−8.0	1398	1439
CPZK3–05							14.7	80.7	0.110	0.512147	0.000005	0.512011	−7.5	1316	1409
CPZK5–04	194	99.9	5.63	0.729100	0.000007	0.71397	13.4	69.1	0.117	0.512170	0.000007	0.512025	−7.2	1371	1381
CPZK5–06							13.8	71.9	0.116	0.512094	0.000013	0.511950	−8.7	1465	1491
Changpu andesites–dacites															
ZK2–02	174	237	2.13	0.720114	0.000010	0.71440	5.78	30.9	0.113	0.511955	0.000007	0.511815	−11.3	1618	1692
ZK2–03	191	65.9	8.41	0.737079	0.000016	0.71448	8.79	40.4	0.132	0.512160	0.000003	0.511997	−7.8	1604	1404
ZK2–04	170	174	2.83	0.722157	0.000009	0.71455	7.82	38.6	0.122	0.512114	0.000003	0.511962	−8.4	1529	1467
ZK2–05	118	366	0.93	0.716814	0.000008	0.71430	7.20	35.6	0.122	0.512079	0.000006	0.511928	−9.1	1579	1517
ZK2–06	108	375	0.83	0.717607	0.000015	0.71537	6.57	33.2	0.120	0.512105	0.000007	0.511957	−8.5	1499	1477
ZK2–07	185	200	2.68	0.721725	0.000014	0.71452	7.09	36.1	0.119	0.512110	0.000008	0.511963	−8.4	1479	1470
Dongkeng rhyolites															
DK1102	224	122	5.33	0.730511	0.000007	0.71620	14.1	67.2	0.127	0.512220	0.000003	0.512062	−6.5	1435	1316
DK1105							25.7	118	0.131	0.512230	0.000003	0.512068	−6.4	1480	1303
DK1106	263	78.3	9.75	0.742125	0.000009	0.71592	10.8	56.6	0.115	0.512204	0.000004	0.512061	−6.5	1299	1330
DK1402	202	140	4.18	0.726138	0.000008	0.71490	8.43	38.4	0.133	0.512154	0.000004	0.511990	−7.9	1635	1412

Chondrite uniform reservoir (CHUR) values ($^{87}Rb/^{86}Sr = 0.0847$, $^{87}Sr/^{86}Sr = 0.7045$; $^{147}Sm/^{144}Nd = 0.1967$, $^{143}Nd/^{144}Nd = 0.512638$) are used for the calculation. $\lambda_{Rb} = 1.42 \times 10$-11 year-1 (Steiger and Jäger, 1977); $\lambda_{Sm} = 6.54 \times 10^{-12}$ year^{-1} (Lugmair and Harti, 1978). The $(^{87}Sr/^{86}Sr)_i$, $(^{143}Nd/^{144}Nd)_i$, ε_{Nd} (t) of the rhyolites from the Changpu and Dongkeng basins were calculated using age of 189 Ma. The details for single-(T_{DM}^{Nd}) or two-stage model age (T_{2DM}^{Nd}) calculations are given by Jahn et al. (1999).

5.4. Tectonic implications

The Early Jurassic igneous rocks in southeastern China remain rare. The few magmatic records from granites and detrital zircons in the coastal region have been interpreted to be evidence for arc magmatism resulted from paleo-Pacific oceanic subduction (Li et al., 2012; Liu et al., 2011). By contrast, studies show that the Early Jurassic magmatism in hinterland south China produced bimodal volcanic sequence, OIB-like basaltic rocks and A-type granitoids which argue for continental extension during this period (Cen et al., 2016; Chen et al., 2005; Gan et al., 2017a, 2017b; He et al., 2010; Li et al., 2003; Li and Li, 2007; Wang et al., 2003; Yu et al., 2010; Zhou et al., 2005; Zhu et al., 2010). As shown in Fig. 12c, the earliest Early Jurassic rhyolites in the Changpu and Dongkeng basins all plot in the within-plate granite field, supporting a continental extensional setting.

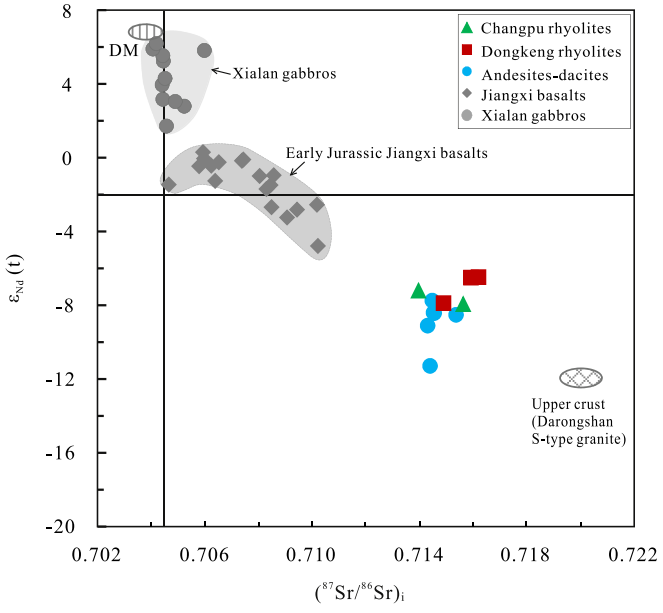

Fig. 13. Initial $\varepsilon_{Nd}(t)$ vs. $(^{87}Sr/^{86}Sr)_i$ diagram for the rhyolites and andesites–dacites from the from the Changpu and Dongkeng basins. The assumed components of the upper crust (ε_{Nd} (190 Ma) = −12, and $(^{87}Sr/^{86}Sr)_i$ (190 Ma) = 0.720), which are similar to the S-type Daronghe granites (Qi et al., 2007; Yu et al., 1999). Data sources: Sr—Nd isotopic data of Early Jurassic Xianlan gabbros from Zhu et al. (2010); Sr—Nd isotopic data of Early Jurassic Jiangxi basalts from Wang et al. (2005) and Cen et al. (2016).

However, the cause for the continental extension is still controversial. Although continental rifting and rift related magmatism can be caused by a mantle plume (Xie et al., 2001), but there is no evidence for its existence at that time. Continental flood basalts, associated dyke swarm and rifting structure are all missing. This model has been very poorly supported and has received little attention. The competing models include post-orogenic continental lithospheric rifting/extension after the Indosinian orogeny (Chen et al., 2008; Wang et al., 2003, 2005), distal lithosphere extension as a result of the subduction of the Paleo-Pacific plate beneath southeastern China (He et al., 2010; Zhou et al., 2006; Zhou and Li, 2000), and in-land lithospheric extension in response to foundering/delamination of the flat subduction of the previously Paleo-Pacific plate beneath southeastern China (Li and Li, 2007). Principally, the first two models relate the earliest Jurassic extension in inland South China to lithospheric extension following Indosinian Orogeny which has been interpreted to record closure of paleo-Tethys Ocean and collision between the South China and Indochina blocks in the Triassic (e.g., Chen et al., 2008; Wang et al., 2003, 2005; Zhou et al., 2006). Both models considered that the subduction of paleo-Pacific oceanic slab beneath did not happen until Jurassic. However, our new results on Changpu high-Mg andesites–dacites suggest that sediments could have been subducted beneath the South China lithosphere before Jurassic.

Although it remains unconstrained when and how the sediment sources of Changpu high-Mg andesites–dacites got subducted, it seems unlikely that they could relate to the closure of the paleo-Tethys which is over 2000 km to the southwest (Metcalfe, 2013). Instead, we suggest that they may be subducted during the flat-slab subduction of an oceanic plateau in the Triassic as that has been proposed by Li and Li (2007). Melting of the subducted sediments followed by melt-mantle interaction in Jurassic finally led to the formation of the Changpu high-Mg andesites–dacites. Although there might be subduction in the Early Jurassic (Liu et al., 2011; Li et al., 2012), spatial-temporal distribution of Jurassic magmatism in hinterland South China implies that it may rather be a response of delamination of the previously subducted oceanic slab that were dehydrated and metamorphosed to eclogitic phases (Li and Li, 2007). Indeed, delamination of the eclogitic oceanic slab and upwelling of asthenosphere have been successfully used to explain the Early Jurassic magmatism, including the

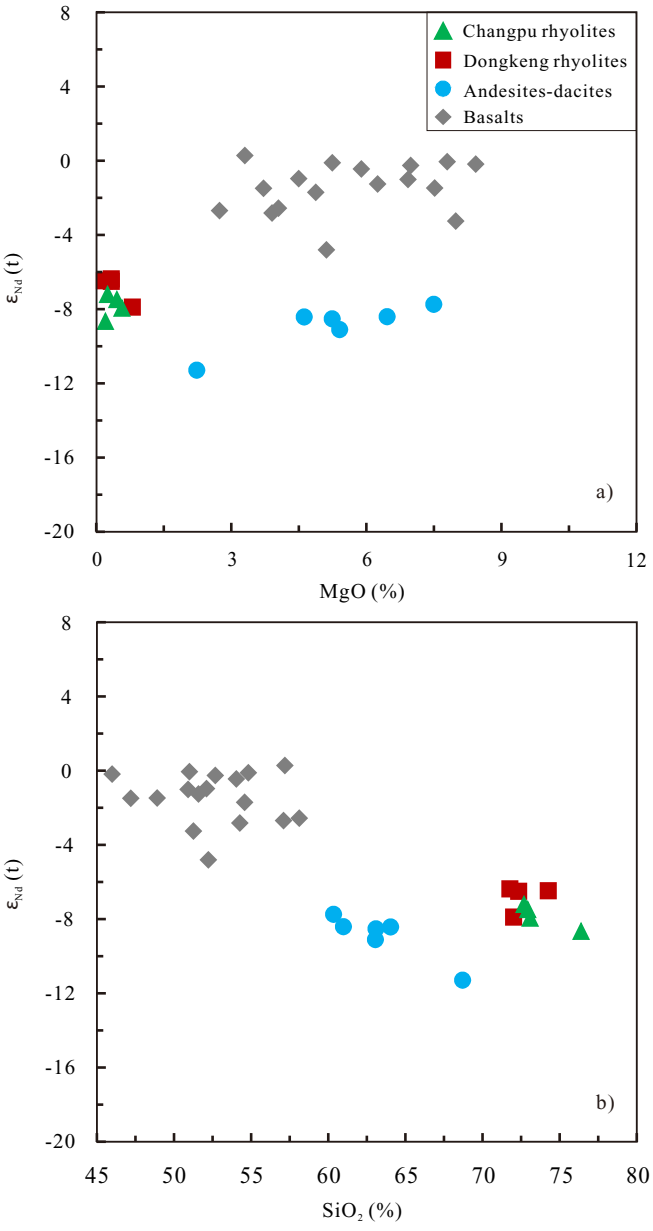

Fig. 14. Plots of (a) initial $\varepsilon_{Nd}(t)$ vs. MgO and (b) $\varepsilon_{Nd}(t)$ vs. SiO_2 showing that mixing between basaltic and rhyolitic magmas from the Changpu and Dongkeng basins cannot explain the geochemical features of the high-Mg andesites–dacites. Data sources: Major elemental (SiO_2 and MgO) and Nd isotopic data of Early Jurassic Jiangxi basalts from Wang et al. (2005) and Cen et al. (2016).

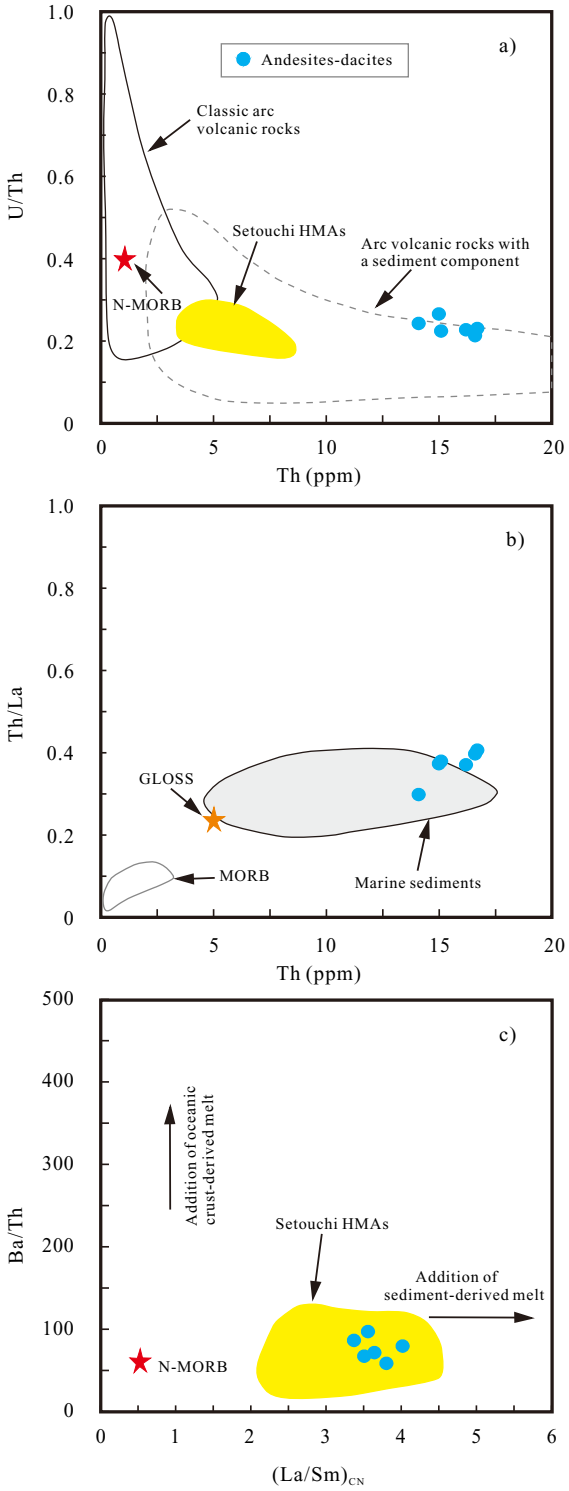

Fig. 15. (a) U/Th-Th diagram (Zeng et al., 2016); (b) Th/La-Th diagram (Liu et al., 2018); (c) Ba/Th-$(La/Sm)_{CN}$ diagram (Labanieh et al., 2012) of the Changpu andesites–dacites. Data sources: sediments from Plank and Langmuir (1998); GLOSS (global subducting sediments) from Plank and Langmuir (1998).

~192–194 Ma Xialan gabbroic intrusion and Wengong A-type granites (Fig. 1b; Zhu et al., 2010), tholeiitic basalts (~190 Ma) in the Changpu and Dongkeng basins (Cen et al., 2016; Wang et al., 2005). To date, however, there is little evidence for melting of subducted materials (Chen et al., 2008). While Cretaceous adakitic rocks in NE south China have been considered as evidence for melting of delaminated slab (Li and Li, 2007), we suggest that discovery of the Changpu high-MgO andesites-tonalites may present as first evidence for melting of subducted sediments.

6. Conclusions

The following conclusions are drawn based on the results from this study:

(1) The CAMECA SIMS zircon U—Pb ages indicate that the rhyolites in the Changpu and Dongkeng basins were erupted at 189–190 Ma, corresponding to the earliest age of the Jurassic period.

(2) The Changpu and Dongkeng rhyolites exhibit the features of A_2-type felsic rocks and have very low $\varepsilon_{Nd}(t)$ (−6.4 to −8.7) coupled by very high $(^{87}Sr/^{86}Sr)_i$ ratios (0.7140 to 0.7162).

Zircons from these rocks show a large range of negative ε_{Hf} (t) (−2.1 to −8.3) and elevated $\delta^{18}O$ values (+7.04 to +9.93‰), consistent with magmas derived from a supracrustal source, plus small amounts of mantle-derived mafic magma.

(3) The Changpu high-Mg andesites-dacites display very low ε_{Nd} (t) (−7.8 to −11.3) coupled by very high $(^{87}Sr/^{86}Sr)_i$ ratios (0.7143 to 0.7154), consistent with magmas formed by interaction between subducted sediment-derived melts and the overlying mantle.

(4) We suggest that the Early Jurassic high-Mg andesites-dacites and rhyolites in the Changpu and Dongkeng basins is related to continental extension as a result of asthenospheric upwelling associated with delamination and foundering of the subducted flat-slab of the Paleo-Pacific oceanic plate beneath the southeastern margin of the South China continental block.

Declaration of Competing Interest

The authors declare that they have no known competing financial interests or personal relationships that could have appeared to influence the work reported in this paper.

Acknowledgments

This study was financially supported by the National Key R&D Program of China (2016YFC0600405) and the National Natural Science Foundation of China (Grants 41572074 and 41273049). We thank X.H. Li, Q.L. Li, Y. Liu and G.Q. Tang for their assistance in SIMS zircon dating and O isotope analysis, H.F. Tang and J.J. Zhu for their assistance in LA–ICP–MS zircon Hf isotope analysis, B. Wang for whole-rock major element analyses by XRF, J. Hu, Y. Huang and G.P. Bao for whole-rock trace element analyses by ICP–MS, F. Xiao and J. Wang for whole-rock Sr—Nd isotopes analyses. We are also grateful that Dr. Chusi Li of Indiana University has helped us not only in the English but also the standard terminology and common expressions used in geology and petrology. The paper benefited from review comments from the editor and two anonymous reviewers.

Appendix A. Supplementary data

Supplementary data to this article can be found online at https://doi.org/10.1016/j.lithos.2020.105403.

References

Bai, Z.J., Zhu, W.G., Zhong, H., Li, C.S., Liao, J.Q., Sun, H.S., 2015. Petrogenesis and tectonic implications of the early Jurassic Fe–Ti oxide-bearing Xialan mafic intrusion in SE China: Constraints from zircon Hf–O isotopes, mineral compositions and whole-rock geochemistry. Lithos 212–215, 59–73.

Blichert-Toft, J., Albarede, F., 1997. The Lu-Hf geochemistry of chondrites and the evolution of the mantle–crust system. Earth Planet. Sci. Lett. 148, 243–258.

Boehnke, P., Watson, E.B., Trail, D., Harrison, T.M., Schmitt, A.K., 2013. Zircon saturation re-revisited. Chem. Geol. 351, 324–334.

Boynton, W.V., 1984. Geochemistry of the rare earth elements: meteorite studies. In: Henderson, P. (Ed.), Rare Earth Element Geochemistry. Elservier, pp. 63–114.

Cen, T., Li, W.X., Wang, X.C., Pang, C.J., Li, Z.X., Xing, G.F., Zhao, X.L., Tao, J.H., 2016. Petrogenesis of early Jurassic basalts in southern Jiangxi Province, South China: Implications for the thermal state of the Mesozoic mantle beneath South China. Lithos 256–257, 311–320.

Chappell, B.W., 1999. Aluminium saturation in I- and S-type granites and the characterization of fractionated haplogranites. Lithos 46, 535–551.

Chen, Z.H., Xing, G.F., 2016. Geochemical and zircon U–Pb–Hf–O isotopic evidence for a coherent Paleoproterozoic basement beneath the Yangtze Block, South China. Precambrian Res. 279, 81–90.

Chen, P.R., Zhou, X.M., Zhang, W.L., Li, H.M., Fan, C.F., Sun, T., Chen, W.F., Zhang, M., 2005. Petrogenesis and significance of early Yanshanian syenite-granite complex in eastern Nanling Range. Science in China Series D (Earth Sciences) 48, 912–924.

Chen, C., Lee, C., Shinjo, R., 2008. Was there Jurassic paleo–Pacific subduction in South China?: constraints from 40Ar/39Ar dating, elemental and Sr–Nd–Pb isotopic geochemistry of the Mesozoic basalts. Lithos 106, 83–92.

Eby, G.N., 1992. Chemical subdivision of the A-type granitoids: petrogenetic and tectonic implications. Geology 20, 641–644.

Eiler, J.M., 2001. Oxygen isotope variations of basaltic lavas and upper mantle rocks. Rev. Mineral. Geochem. 43, 319–364.

Gan, C.S., Wang, Y.J., Zhang, Y.Z., Zhang, J., 2017a. The earliest Jurassic A-type granite in the Nanling Range of southeastern South China: petrogenesis and geological implications. International Geology Review 59, 274–292.

Gan, C.S., Wang, Y.J., Qian, X., Bi, M.W., He, H.Y., 2017b. Constraints of the Xialan gabbroic intrusion in the Eastern Nanling Range on the early Jurassic intra-continental extension in eastern South China. J. Asian Earth Sci. 145, 576–590.

Gao, S., Rudnick, R.L., Yuan, H.L., Liu, X.M., Liu, Y.S., Xu, W.L., Ling, W.L., Ayers, J., Wang, X.C., Wang, Q.H., 2004. Recycling lower continental crust in the North China craton. Nature 432, 892–897.

Griffin, W.L., Wang, X., Jackson, S.E., Pearson, N.J., O'Reilly, S.Y., Xu, X., Zhou, X., 2002. Zircon chemistry and magma mixing, SE China: in-situ analysis of Hf isotopes, Tonglu and Pingtan igneous complexes. Lithos 61, 237–269.

He, Z.Y., Xu, X.S., 2012. Petrogenesis of the Late Yanshanian mantle-derived intrusions in southeastern China: Response to the geodynamics of paleo-Pacific plate subduction. Chem. Geol. 328, 208–221.

He, Z.Y., Xu, X.S., Niu, Y.L., 2010. Petrogenesis and tectonic significance of a mesozoic granite–syenite–gabbro association from inland South China. Lithos 119, 621–641.

Huang, H.Q., Li, X.H., Li, W.X., Li, Z.X., 2011. Formation of high $\delta^{18}O$ fayalite-bearing A-type granite by high temperature melting of granulitic metasedimentary rocks, southern China. Geology 39, 903–906.

Jahn, B.M., Zhou, X.H., Li, J.L., 1990. Formation and tectonic evolution of southeastern China and Taiwan: isotopic and geochemical constraints. Tectonophysics 183, 145–160.

Jahn, B.M., Wu, F.Y., Lo, C.H., Tsai, C.H., 1999. Crust-mantle interaction induced by deep subduction of the continental crust: geochemical and Sr-Nd isotopic evidence from post-collisional mafic–ultramafic intrusions of the northern Dabie complex, central China. Chem. Geol. 157, 119–146.

Ji, C.Y., Wu, J.H., 2010. The SHRIMP zircon U–Pb dating of felsic volcanic rocks and its geological significance from Yutian group in southern Jiangxi. Journal of East China Institute of Technology 33 (02), 131–138 (in Chinese).

Jiao, S.J., Li, X.H., Huang, H.Q., Deng, X.D., 2015. Metasedimentary melting in the formation of charnockite: petrological and zircon U-Pb-Hf-O isotope evidence from the Darongshan S-type granitic complex in southern China. Lithos 239, 217–233.

Kelemen, P.B., Yogodzinski, G.M., Scholl, D.W., 2003. Along-strike variation in the Aleutian island arc: genesis of high $Mg^{\#}$ andesite and implications for continental crust. In: Eiler, J. (Ed.), Inside the Subduction Factory. American Geophysical Union Geophysical Monograph 138, pp. 223–276.

Kemp, A.I.S., Hawkesworth, C.J., Foster, G.L., Paterson, B.A., Woodhead, J.D., Hergt, J.M., Gray, C.M., 2007. Magmatic and crustal differentiation history of granitic rocks from Hf–O isotopes in zircon. Science 315, 980–983.

Kerr, A., Fryer, B.J., 1993. Nd isotope evidence for crust mantle interaction in the generation of A-type granitoid suites in Labrador, Canada. Chem. Geol. 104, 39–60.

Labanieh, S., Chauvel, C., Germa, A., Quidelleur, X., 2012. Martinique: a clear case for sediment melting and slab dehydration as a function of distance to the trench. J. Petrol. 53, 2441–2464.

Le Bas, M.J., Streckeisen, A.L., 1991. The IUGS systematics of igneous rocks. Journal of the Geological Society London 148, 825–833.

Li, X.H., 2000. Cretaceous magmatism and lithospheric extension in Southeast China. J. Asian Earth Sci. 18, 293–305.

Li, Z.X., Li, X.H., 2007. Formation of the 1300-km-wide intracontinental orogen and postorogenic magmatic province in Mesozoic South China: a flat-slab subduction model. Geology 35, 179–182.

Li, X.H., Sun, M., Wei, G.J., Liu, Y., Lee, C.Y., Malpas, J., 2000. Geochemical and Sm–Nd isotopic study of amphibolites in the Cathaysia Block, southeastern China: evidence for an extremely depleted mantle in the paleoproterozoic. Precambrian Res. 102, 251–262.

Li, X.H., Chen, Z.G., Liu, D.Y., Li, W.X., 2003. Jurassic gabbro-granite-syenite suites from Southern Jiangxi Province, SE China: age, origin, and tectonic significance. International Geology Review 45, 898–921.

Li, X.H., Li, Z.X., Li, W.X., Wang, Y.J., 2006. Initiation of the Indosinian orogeny in South China: evidence for a Permian magmatic arc on the Hainan Island. J. Geol. 114, 341–353.

Li, X.H., Li, Z.X., Li, W.X., Liu, Y., Yuan, C., Wei, G.J., Qi, C.S., 2007. U-Pb zircon, geochemical and Sr-Nd-Hf isotopic constraints on age and origin of Jurassic I- and A-type granites from central Guangdong, SE China: a major igneous event in response to foundering of a subducted flat-slab? Lithos 96, 186–204.

Li, X.H., Li, W.X., Wang, X.C., Li, Q.L., Liu, Y., Tang, G.Q., 2009a. Role of mantle-derived magma in genesis of early Yanshanian granites in the Nanling Range, South China: in situ zircon Hf-O isotopic constraints. Science in China Series D: Earth Sciences 52, 1262–1278.

Li, X.H., Liu, Y., Li, Q.L., Guo, C.H., Chamberlain, K.R., 2009b. Precise determination of phanerozoic zircon Pb/Pb age by multi-collector SIMS without external standardization. Geochemistry Geophysics Geosystems 10, Q04010. https://doi.org/10.1029/2009GC002400.

Li, Z.X., Li, X.H., Chung, S.L., Lo, C.H., Xu, X.S., Li, W.X., 2012. Magmatic switch-on and switch-off along the South China continental margin since the Permian: transition from an Andean-type to a Western Pacific-type plate boundary. Tectonophysics 532–535, 271–290.

Li, X.H., Tang, G.Q., Gong, B., Yang, Y.H., Hou, K.J., Hu, Z.C., Li, Q.L., Liu, Y., Li, W.X., 2013. Qinghu zircon: a working reference for microbeam analysis of U-Pb age and Hf and O isotopes. Chin. Sci. Bull. 58, 4647–4654.

Liu, Q., Yu, J.H., Su, B., Wang, Q., Tang, H.F., Xu, H., Cui, X., 2011. Discovery of the 187 Ma granite in Jincheng area, Fujian Province: constraint on early Jurassic tectonic evolution of southeastern China. Acta Petrologica Sinica 27, 3575–3589.
Liu, W.L., Huang, Q.T., Gu, M., Zhong, Y., Zhou, R.J., Gu, X.D., Zheng, H., Liu, J.N., Lu, X.X., Xia, B., 2018. Origin and tectonic implications of the Shiquanhe high-Mg andesite, western Bangong suture, Tibet. Gondw. Res. 60, 1–14.
Ludwig, K.R., 2001. Users manual for Isoplot/Ex rev. 2.49. Berkeley Geochronology Centre Special Publication. No. 1a 56 pp.
Lugmair, G.W., Harti, K., 1978. Lunar initial $^{143}Nd/^{144}Nd$: differential evolution of the lunar crust and mantle. Earth Planet. Sci. Lett. 39, 349–357.
McCarron, J.J., Smellie, J.L., 1998. Tectonic implications of fore-arc magmatism and generation of high-magnesian andesites: Alexander Island, Antarctica. J. Geol. Soc. London 155 (2), 269–280.
Meng, L.F., Li, Z.X., Chen, H.L., Li, X.H., Wang, X.C., 2012. Geochronological and geochemical results from Mesozoic basalts in southern South China Block support the flat-slab subduction model. Lithos 132–133, 127–140.
Metcalfe, I., 2013. Gondwana dispersion and Asian accretion: tectonic and palaeogeographic evolution of eastern Tethys. J. Asian Earth Sci. 66, 1–33.
Pearce, J.A., Harris, N.B.W., Tindle, A.G., 1984. Trace element discrimination diagrams for the tectonic interpretation of granitic rocks. J. Petrol. 25, 956–983.
Plank, T., Langmuir, C.H., 1998. The chemical composition of subducting sediment and its consequences for the crust and mantle. Chem. Geol. 145, 325–394.
Qi, L., Hu, J., Gregoire, D.C., 2000. Determination of trace elements in granites by inductively coupled plasma mass spectrometry. Talanta 51, 507–513.
Qi, C.S., Deng, X.G., Li, W.X., Li, X.H., Yang, Y.H., Xie, L.W., 2007. Origin of the Darongshan-Shiwandashan S-type ganiteoid belt from southeastern Guangxi: geochemical and Sr-Nd-Hf isotopic constraints. Acta Petrol. Sin. 23, 403–412.
Qian, Q., Hermann, J., 2010. Formation of high-Mg diorites through assimilation of peridotite by monzodiorite magma at crustal depths. J. Petrol. 51, 1381–1416.
Rickwood, P.C., 1989. Boundary lines within petrologic diagrams which use oxides of major and minor elements. Lithos 22, 247–263.
Rudnick, R.L., Gao, S., 2003. Composition of the continental crust. Treatise on Geochemistry. 3, pp. 1–64.
Shimoda, G., Tatsumi, Y., Nohda, S., Ishizaka, K., Jahn, B.M., 1998. Setouchi high-Mg andesites revisited: geochemical evidence for melting of subducting sediments. Earth Planet. Sci. Lett. 160, 479–492.
Söderlund, U., Patchett, P.J., Vervoort, J.D., Isachsen, C.E., 2004. The Lu-176 decay constant determined by Lu-Hf and U–Pb isotope systematics of Precambrian mafic intrusions. Earth Planet. Sci. Lett. 219, 311–324.
Steiger, R.H., Jäger, E., 1977. Subcommission on geochronology: convention on the use of decay constants in geo- and cosmochronology. Earth Planet. Sci. Lett. 36, 359–362.
Streck, M.J., Leeman, W.P., Chesley, J., 2007. High-magnesian andesite from Mount Shasta: a product of magma mixing and contamination, not a primitive mantle melt. Geology 35 (4), 351–354.
Sun, S.-S., McDonough, W.F., 1989. Chemical and isotopic systematics of oceanic basalts: implications for mantle composition and processes. In: Saunders, A.D., Norry, M.J. (Eds.), Magmatism in the Ocean Basins. 42. Geological Society, London, Special Publications, pp. 313–345.
Tang, G.J., Wang, Q., 2010. High-Mg andesites and their geodynamic implications. Acta Petrol. Sin. 26, 2495–2512.
Tang, H.F., Zhao, Z.Q., Han, R.S., Han, Y.J., Su, Y.P., 2008. Primary Hf isotopic study on zircons from the A-type granites in Eastern Junggar of Xinjiang, northwest China. Acta Mineralogica Sinica 28, 335–342.
Tatsumi, Y., 2001. Geochemical modeling of partial melting of subducting sediments and subsequent melt-mantle interaction: generation of high-Mg andesites in the Setouchi volcanic belt, Southwest Japan. Geology 29, 323–326.
Turner, S.P., Foden, J.D., Morrison, R.S., 1992. Derivation of some A-type magmas by fractionation of basaltic magma: an example from the Padthaway Ridge, South Australia. Lithos 28, 151–179.
Turner, S., Hawkesworth, C., Calsteren, P.V., Heath, E., Macdonald, R., Black, S., 1996. U-series isotopes and destructive plate margin magma genesis in the Lesser Antilles. Earth Planet. Sci. Lett. 142, 191–207.
Valley, J.W., Lackey, J.S., Cavosie, A.J., Clechenko, C.C., Spicuzza, M.J., Basei, M.A.S., Bindeman, I.N., Ferreira, V.P., Sial, A.N., King, E.M., Peck, W.H., Sinha, A.K., Wei, C.S., 2005. 4.4 billion years of crustal maturation: oxygen isotope ratios of magmatic zircon. Contrib. Mineral. Petrol. 150, 561–580.
Vervoort, J.D., Blichert-Toft, J., 1999. Evolution of the depleted mantle: Hf isotope evidence from juvenile rocks through time. Geochim. Cosmochim. Acta 63, 533–556.
Wang, Y.J., Fan, W.M., Guo, F., Peng, T.P., Li, C.W., 2003. Geochemistry of mesozoic mafic rocks adjacent to the Chenzhou-Linwu fault, South China: implications for the lithospheric boundary between the yangtze and cathaysia blocks. International Geology Review 45, 263–286.
Wang, Y.J., Fan, W.M., Peng, T.P., Guo, F., 2005. Elemental and Sr–Nd isotopic systematics of the early Mesozoic volcanic sequence in southern Jiangxi Province, South China: petrogenesis and tectonic implications. International Journal of Earth Sciences 94, 53–65.
Whalen, J.B., Currie, K.L., Chappell, B.W., 1987. A-type granites: geochemical characteristics, discrimination and petrogenesis. Contrib. Mineral. Petrol. 95, 407–419.
Wood, B.J., Turner, S.P., 2009. Origin of primitive high-Mg andesite: constraints from natural examples and experiments. Earth Planet. Sci. Lett. 283, 59–66.
Woodhead, J., Hergt, J., Shelley, M., Eggins, S., Kemp, R., 2004. Zircon Hf-isotope analysis with an excimer laser, depth profiling, ablation of complex geometries, and concomitant age estimation. Chem. Geol. 209, 121–135.
Wu, J.H., Zhou, W.X., Zhang, B.T., 2000. Stratigraphic division and geologic era of Mesozoic era volcanic rock series in South Jiangxi–North Guangdong. Geological Review 46, 362–370 (in Chinese).
Xie, G.Q., Hu, R.Z., Zhao, J.H., Jiang, G.H., 2001. Mantle plume and the relationship between it and mesozoic large-scale metallogenesis in southeastern China: a preliminary discussion. Geotectonica et Metallogenia 25, 179–186 (in Chinese).
Xu, J.F., Shinjo, R., Defant, M.J., Wang, Q.A., Rapp, R.P., 2002. Origin of Mesozoic adakitic intrusive rocks in the Ningzhen area of East China: partial melting of delaminated lower continental crust? Geology 30 (12), 1111–1114.
Yang, J.H., Wu, F.Y., Wilde, S.A., Xie, L.W., Yang, Y.H., Liu, X.M., 2007. Tracing magma mixing in granite genesis: in situ U–Pb dating and Hf-isotope analysis of zircons. Contrib. Mineral. Petrol. 153, 177–190.
Yogodzinski, G.M., Volynets, O.N., Koloskov, A.V., Seliverstov, N.I., Matvenkov, V.V., 1994. Magnesian andesites and the subduction component in a strongly calc-alkaline series at Piip Volcano, Far Western Aleutians. J. Petrol. 35, 163–204.
Yu, J.S., Gui, X.T., Yuan, C., 1999. The characteristics of isotopes geochemistry of darongshan granitoid suite, Guangxi. Guangxi Geology 12, 1–6 (in Chinese).
Yu, J.H., Wang, L.J., Griffin, W.L., O'Reilly, S.Y., Zhang, M., Li, C.-Z., Shu, L.S., 2009. A Paleoproterozoic orogeny recorded in a long-lived cratonic remnant (Wuyishan terrane), eastern Cathaysia Block, China. Precambrian Res. 174, 347–363.
Yu, X.Q., Wu, G.G., Zhao, X., Gao, J.F., Di, Y.J., Zheng, Y., Dai, Y.P., Li, C.L., Qiu, J.T., 2010. The Early Jurassic tectono-magmatic events in southern Jiangxi and northern Guangdong provinces, SE China: Constraints from the SHRIMP zircon U–Pb dating. J. Asian Earth Sci. 39, 408–422.
Zeng, Y., Chen, J., Xu, J., Wang, B., Huang, F., 2016. Sediment melting during subduction initiation: geochronological and geochemical evidence from the Darutso high-Mg andesites within ophiolite melange, Central Tibet. Geochemistry Geophysics Geosystems 17, 4859–4877.
Zhang, B.T., Chen, P.R., Kong, X.G., 2002. Rb-Sr chronology of bimodal volcanic rocks of the Yutian Group in the Linjiang basion, southern Jiangxi. Geology in China 29, 352–354 (in Chinese).
Zhou, X.M., Li, W.X., 2000. Origin of late Mesozoic igneous rocks in Southeastern China: implications for lithosphere subduction and underplating of mafic magmas. Tectonophysics 326, 269–287.
Zhou, J.C., Jiang, S.Y., Wang, X.L., Yang, J.H., Zhang, M.Q., 2005. Re–Os isochron age of Fankeng basalts from Fujian of SE China and its geological significance. Geochem. J. 39, 497–502.
Zhou, X.M., Sun, T., Shen, W.Z., Shu, L.S., Niu, Y.L., 2006. Petrogenesis of mesozoic granitoids and volcanic rocks in South China: a response to tectonic evolution. Episodes 29, 26–33.
Zhu, W.G., Zhong, H., Li, X.H., He, D.F., Song, X.Y., Ren, T., Chen, Z.Q., Sun, H.S., Liao, J.Q., 2010. The early Jurassic mafic–ultramafic intrusion and A-type granite from northeastern Guangdong, SE China: Age, origin, and tectonic significance. Lithos 119, 313–329.